Phage-encoded sRNA counteracts xenogenic silencing in pathogenic *E. coli*

Pranita Poudyal[1], Brandon Sy[1], Daniel G. Mediati[2], Michael Payne[1], Vibhuti Nandel[1], Dougall Norris[1], Sean McAteer[3], Asim Ullah[3], Serena Li[1], Lawrence Menz[1], Shafagh A. Waters[4], Timothy J. Dallman[5], Mathew Baker[1], Ruiting Lan[1], David Gally[3], Jai Tree[1]

[1]School of Biotechnology and Biomolecular Sciences, UNSW, Sydney, Australia
[2]Australian Institute for Microbiology and Infection, University of Technology Sydney, Sydney, Australia
[3]The Roslin Institute, Division of Bacteriology, University of Edinburgh, Edinburgh, United Kingdom
[4]School of Medical Sciences, Faculty of Medicine and Health, UNSW, Sydney, Australia
[5]WHO Hub for Pandemic and Epidemic Intelligence, WHO Health Emergency Preparedness & Response Programme, World Health Organization, Berlin, Germany

ABSTRACT

Horizontal gene transfer introduces foreign DNA that can disrupt cellular processes and is therefore subject to xenogenic silencing by nucleoid-associated proteins such as H-NS and Hha. In Enterohaemorrhagic *Escherichia coli* (EHEC), prophages make up a large fraction of the accessory genome and encode many virulence factors, yet to be expressed they must overcome this silencing. We identify a prophage-encoded small RNA (sRNA), HnrS, that functions as an anti-silencing factor by targeting the H-NS paralogue Hha. HnrS is a short (66-nt) sRNA present in multiple copies (up to nine) in EHEC and Enteropathogenic *Escherichia coli* (EPEC) genomes and is enriched in *E. coli* strains that carry the locus of enterocyte effacement (LEE^+). We show that HnrS directly base-pairs with the ribosome-binding site of the *hha* mRNA, repressing its translation and thereby reducing Hha-enhanced H-NS silencing. This counter-silencing de-represses the LEE type III secretion system and concomitantly represses motility. Transcriptomic profiling further revealed that HnrS indirectly activates genes involved in nitrate/nitrite respiration and nitric oxide resistance, metabolic pathways that contribute to survival in the inflamed gastrointestinal tract. Deletion of *hnrS* reduced expression of nitrate reductase genes and impaired actin pedestal formation on host epithelial cells. Our results indicate that prophage-encoded, multicopy *hnrS* provides a counter-silencing mechanism that reduces Hha–H-NS repression at specific virulence loci. This likely enables expression of horizontally acquired genes without broadly disrupting the core H-NS regulon. HnrS illustrates how mobile genetic elements deploy sRNAs to counteract xenogenic silencing and promote virulence gene expression, enhancing colonisation of the host.

Importance statement

Horizontally acquired genes are often silenced to protect bacterial genomes, but this defence also limits the expression of new traits. We identify a prophage-encoded small RNA, HnrS, that counteracts this restriction by repressing the xenogenic silencer Hha, lifting Hha–H-NS-mediated repression of virulence and metabolic genes. HnrS activates the locus of enterocyte effacement, nitrate/nitrite respiration, and nitric oxide resistance—pathways that help *E. coli* survive and colonise the inflamed gut. Our findings reveal an RNA-based counter-silencing mechanism encoded by mobile genetic elements, showing how phages can reprogram bacterial regulatory networks to promote adaptation and pathogenicity.

60 **INTRODUCTION**

61 Horizontal gene transfer (HGT) plays a central role in bacterial evolution, enabling the
62 acquisition of genes that confer new functions such as antibiotic resistance and virulence.
63 However, incoming DNA can also disrupt cellular processes or impose metabolic costs and is
64 therefore restricted by multiple layers of genome defence. The most frequent include
65 restriction–modification systems, CRISPR-Cas, and cyclic oligonucleotide-based antiphage
66 signalling systems (CBASS), among an expanding repertoire of defence systems (1).

67 Foreign DNA that evades initial restriction can be integrated into the genome but is frequently
68 detrimental to host fitness (2). In *Enterobacteriaceae*, foreign DNA is often more AT-rich than
69 the host genome and is transcriptionally silenced by the nucleoid-associated protein H-NS,
70 which binds to AT-rich regions and forms oligomeric complexes that repress transcription (3-
71 8). This process—termed xenogenic silencing—enables bacteria to tolerate the presence of
72 foreign genes without incurring their deleterious effects (2, 9-11). Deletion of *hns* is lethal in
73 several pathogens (12-15) underscoring the role of H-NS in suppressing deleterious gene
74 expression.

75 For horizontally-acquired genes to be retained under positive selection they must be expressed.
76 Activation can occur through specific transcription factors that counteract H-NS-mediated
77 silencing in response to environmental cues (15). A broader anti-silencing strategy is used by
78 bacteriophage T7 that encodes a protein (gene 5.5) that forms heterodimers with H-NS,
79 reducing its DNA-binding activity and enabling phage transcription (16). However, global
80 interference with H-NS is likely to de-repress a broad range of largely detrimental genes and
81 be costly to the host.

82 H-NS silencing is selectively enhanced at virulence loci by Hha, a small H-NS paralogue that
83 lacks a DNA-binding domain but forms heterodimers with H-NS to increase its affinity for
84 specific targets (17). Hha appears to enhance H-NS activity on foreign genes, particularly at
85 virulence-associated islands, without affecting the expression of H-NS-regulated genes in the
86 core genome (17, 18). Structural and biochemical analysis of the Hha-H-NS heterodimer
87 indicates that Hha coats the H-NS oligomerisation domain and presents a positive surface that
88 increases DNA binding (18).

In Enterohaemorrhagic *Escherichia coli* (EHEC), horizontal gene transfer has introduced over 1.5 Mb of new genetic material, including 19 prophages that carry many key virulence factors (19, 20). We previously showed that these regions are rich in small regulatory RNAs (sRNAs), several of which contribute to virulence gene expression (21-23). Here, we identify an sRNA, HnrS, encoded on prophages and present in up to nine copies in attaching and effacing *E. coli* strains that encode the locus of enterocyte effacement (LEE+). We demonstrate that HnrS directly base pairs with the ribosome binding site of *hha* mRNA to represses *hha* expression, partly relieving Hha-H-NS-mediated silencing. This results in upregulation of the LEE encoded type 3 secretion system and repression of motility. In addition, HnrS promotes the expression of genes involved in nitric oxide resistance and nitrate/nitrite respiration—key adaptations for survival in the inflamed gastrointestinal tract (24-26). Together, these data support a model in which multiple prophage-encoded copies of HnrS provide a dosage-tunable mechanism to counteract xenogenic silencing at specific virulence loci, promoting virulence gene expression and host colonisation while avoiding broad de-repression of the core H-NS regulon.

103 **RESULTS**

104 **HnrS is a multicopy small RNA encoded on prophages**

105 In EHEC strains horizontally-acquired pathogenicity islands encode the majority of virulence
106 factors, as well as regulators that tune their expression. In our previous analysis of the sRNA
107 interactome in EHEC str. Sakai we identified several sRNAs within the pathogenicity islands
108 (S-loops) with abundant mRNA interactions (27), suggesting a role in virulence. Among the
109 most abundant were three identical copies of a single sRNA – designated EcOnc10, EcOnc11,
110 and EcOnc12 – encoded within the prophages Sp9, Sp10, and Sp12 respectively. We here
111 rename these sRNA HnrS (Hha-negative regulatory small RNA). We had previously identified
112 these sRNAs through their Hfq-binding (21) indicating that they are Hfq-associated sRNA
113 (**Figure 1A**). To precisely map the 5' and 3' ends of the sRNAs, we analysed dRNA-seq and
114 Term-seq data for EHEC str. Sakai. All three loci share identical 5' and 3' ends and produced
115 a 66-nt sRNA transcript terminated by an intrinsic Rho-independent terminator (**Figure 1A**).
116 Northern blot analysis supported transcription of a 66-nt sRNA and indicated that it
117 accumulates during early stationary phase in both T3SS-inducing MEM-HEPES and minimal
118 M9 media (**Figure 1B**), similar to the Stx phage sRNA, StxS (28)
119
120 To assess the distribution of HnrS across *E. coli* pathotypes, we searched for copies within
121 3,230 *E. coli* genomes in NCBI and assigned pathotypes from characteristic virulence genes
122 (Methods & Supplementary Information)(29, 30). We identified *hnrS* predominantly in EHEC
123 and EPEC pathotypes (98.01%), with a minor representation in uropathogenic (0.82%) and
124 unclassified (1.17%) *E. coli* strains (**Figure 2A**). Shiga toxin genes (*stx1* and s*tx 2* that partly
125 characterise EHEC) were significantly enriched in the *hnrS* encoding strains (p<0.0001), as
126 was the LEE that facilitates attaching and effacing lesion formation in EHEC and EPEC
127 (p<0.0001, Fishers exact test).
128
129 The Sakai strain of EHEC has been extensively studied and harbours three copies of HnrS on
130 distinct prophages. To assess variation in gene dosage across strains, we estimated relative *hnrS*
131 copy number from normalised sequencing read depth **(Figure 2A-B**). Specifically, the
132 coverage of *hnrS* was normalised against the mean coverage of six conserved housekeeping
133 genes (*arpA*, *trpA*, *uidA*, *rrl*, *tspE4*, and *fyuA*) to yield a relative read coverage that
134 approximates copy number. The median relative coverage for *hnrS* among O157:H7 strains
135 was approximately 2-fold, with the highest exceeding 7-fold in one isolate **(Figure 2C**).

136 Among EHEC serotypes, O177:H25 and O157:H7 exhibited a significantly higher *hnrS*
137 relative coverage, with some isolates encoding 9-fold more *hnrS* relative to the housekeeping
138 gene controls. Because O157:H7 is the serotype most commonly associated with human
139 infection, we asked whether increased *hnrS* copy number is associated with human infection.
140 Comparing isolates from human infections versus cattle (reservoir) measured as normalised
141 read depth (FPKM [Fragments per kilobase of transcript per million mapped reads]) (31),
142 indicated that the median relative coverage for human isolates trended higher but this difference
143 was not statistically significant (**Figure 2D**).
144
145 Given recent reports of bacteriophage sRNAs that promote phage survival (32, 33), we asked
146 whether HnrS is prophage-encoded in other EHEC and EPEC strains. We used PHASTER
147 analysis to identify prophage regions in a subset of strains. In each EPEC and EHEC strain, a
148 single copy of HnrS was encoded within the late genes of an independent prophage element
149 (**Supplementary Figure 1**). These results indicate that HnrS is acquired by insertion of
150 prophages into the genome, and that multiple copies arise from the acquisition of distinct
151 prophages.
152
153 **HnrS represses the xenogenic DNA silencer, Hha**
154 The acquisition of multiple copies of *hnrS* on phage suggests that the sRNA contributes to
155 phage and/or host fitness. Using our previously published sRNA interactome data (RNase E-
156 CLASH) (27), we identified target mRNAs for HnrS. The most abundant interaction for HnrS
157 was with the toxin-antitoxin system, *mazEF* (129-hybrids, FDR=0). The *mazEFG* operon
158 comprises the antitoxin *mazE* and the toxin *mazF*, followed by *mazG*, which encodes a
159 nucleoside triphosphate pyrophosphohydrolase thought to modulate programmed cell death
160 and stress adaptation (34) . HnrS has perfect complementary with the last 15-nt the *mazF*
161 coding sequence (**Supplementary Figure 2A)**. We confirmed that HnrS interacts with the
162 *mazF* coding sequence *in vitro* using EMSA (**Supplementary Figure 2B-C**). MazEF has
163 previously been proposed to confer resistance to phage P1 and T4 (34, 35), we therefore tested
164 whether HnrS may antagonise this phage defence system. We did not observe P1 or T4
165 susceptibility in a Δ*mazEFG* strain and overexpression of HnrS in commensal *E. coli* str.
166 MG1655 (that lacks the *hnrS*-encoding prophages) did not confer phage susceptibility
167 (**Supplementary Figure 2D**). Notably, our strain backgrounds and Δ*mazEFG* construct differ
168 from those previously reported and may explain our divergent results (34, 35). We next asked
169 if HnrS can suppress MazEF toxicity. Overexpression of *mazEF* was toxic to *E. coli* str.

170 MG1655, but co-expression of HnrS had no appreciable effect on MazEF toxicity
171 (**Supplementary Figure 3A**). To understand if HnrS might direct processing of the *mazFG*
172 intergenic region or regulate downstream *mazG*, we constructed a *mazFG*-GFP translational
173 fusion and monitored fluorescence in the presence or absence of HnrS. MazG'-GFP was
174 modestly reduced (~13%), a change we do not consider biologically meaningful
175 (**Supplementary Figure 3B**). Together these data suggest that while HnrS interacts with *mazF*
176 *in vivo* and *in vitro*, it does not measurably modulate MazEF abundance or promote T4 or P1
177 susceptibility in *E. coli* str. MG1655. We note that non-canonical sRNA functions have
178 recently been uncovered (36), leaving open alternative mechanisms not captured by our assays.
179
180 To identify functional targets of HnrS, we constructed GFP translational fusions to the
181 remaining HnrS-mRNA interactions identified by RNase E-CLASH (FDR<0.2 or hybrid
182 count>2). Two mRNAs were significantly regulated by HnrS, the transcription factor AsnC
183 was upregulated (1.32-fold, p=0.03) and the xenogenic silencer Hha was repressed 10-fold
184 (p<0.0001) (**Figure 3A-B**). To confirm that HnrS is a direct repressor of Hha we introduced
185 compensatory mutations into the seed-region of HnrS and *hha* 5' UTR. Single point mutations
186 in either the sRNA or mRNA seed disrupted repression, whereas the compensatory double
187 mutant restored repression, indicating that regulation was dependant on direct base-pairing
188 between HnrS and *hha* RNAs (**Figure 3C-D**).
189
190 Hha forms a complex with H-NS and promotes silencing of predominately horizontally-
191 acquired genes and virulence genes in *E. coli* and *Salmonella* (17, 18, 37). Our data indicate
192 that the prophage-encoded sRNA HnrS represses Hha, suggesting that it acts to counter
193 xenogenic silencing.
194
195 **HnrS represses motility in commensal and enterohaemorrhagic *E. coli***
196 Hha positively regulates motility in *E. coli* and *Salmonella* through activation of the master
197 flagellar regulator FlhDC (38, 39). We initially quantified Hha regulation of motility in EHEC
198 str. Sakai. Single-cell swim speed was measured for the wild type, Δ*hha*, and the complemented
199 mutant (Δ*hha* pBR322::*hha*) using phase-contrast microscopy (**Figure 4A**). Consistent with
200 earlier reports, deletion of *hha* dramatically reduced swim speed in EHEC str. Sakai (4.7-fold,
201 p<0.0001) and was restored in the complemented background.
202

203 To assess whether HnrS is able to repress motility, a HnrS expression construct (pZE12::*hnrS*)
204 was moved into the hypermotile commensal *E. coli* str. RP437 (that lacks the *hnrS*-encoding
205 prophages). Expression of HnrS in the commensal background significantly reduced motility
206 compared to a scrambled sRNA control (**Figure 4B**), consistent with HnrS repression of *hha*.
207
208 To simultaneously knockdown all three HnrS copies in EHEC we used CRISPR interference
209 (CRISPRi). HnrS was not detectable after knockdown by Northern blot at early stationary
210 phase indicating efficient knockdown (**Figure 4C**). CRISPRi knockdown of HnrS significantly
211 increased motility (1.9-fold, p=0.0023), mirroring the overexpression phenotype in commensal
212 *E. coli* str. RP437 (**Figure 4D**).
213
214 Because the Δ*hha* mutant is essentially non-motile, epistasis could not be assessed by double
215 mutant analysis. However, our results are consistent with HnrS repressing motility through Hha
216 that is required to activate the FlhDC regulatory cascade.
217
218 **HnrS promotes T3SS in EHEC**
219 Expression of the T3SS is essential for EHEC colonisation of both ruminants and humans and
220 is silenced by Hha-H-NS (40-43). Given that the great majority (98.01%) of *hnrS*-encoding *E.*
221 *coli* are also LEE+, we speculated that a major selective pressure for maintaining multiple
222 copies of HnrS may be de-repression of the LEE to promote colonisation. We initially
223 confirmed that Hha represses the T3SS in our low-secretion EHEC str. Sakai background and
224 in a high-secretion strain, TUV93-0 (a derivative of EDL933 lacking both *stx*-encoding
225 phages). Deletion of *hha* in both strain backgrounds resulted in strong de-repression of T3SS
226 that was restored to wild type levels in the complemented strain (**Figure 5A**).
227
228 The T3SS is positively regulated by the master regulator Ler encoded at the start of the LEE1
229 operon. Using GFP transcriptional fusions to the LEE1 (*ler*), LEE5 (*tir*), and LEE4 (*sepL*)
230 promoters, we quantified promoter activity in the Δ*hha* backgrounds (**Supplementary Figure**
231 **4**). Consistent with earlier work (44), deletion of *hha* de-repressed the LEE1 and LEE5
232 promoters, but not the LEE4 promoter in EHEC str. Sakai and was restored to wild type in the
233 *hha* complementation strain.
234
235 CRISPRi knockdown of HnrS reduced the amount of T3S in both strain backgrounds, although
236 baseline secretion levels were lower in the presence of the CRISPRi construct. In Sakai,

237 laddering of cytoplasmic proteins from *stx*-phage lysis obscured identification of the T3SS
238 proteins (**Figure 5B**). To quantify T3SS proteins in the CRISPRi expressing background we
239 used antibodies against the T3SS needle tip, EspD (**Figure 5C**). EspD was de-repressed 2.3-
240 fold, (p<0.0001) in the EHEC str. Sakai Δ*hha* background and restored to wild type in the
241 complemented strain. Conversely, *hnrS* knockdown significantly reduced EspD expression
242 1.7-fold (p<0.0001) in the high secretion strain TUV93-0 and 1.1-fold (p=0.0092) in the low
243 secretion strain Sakai (**Figure 5D**).
244
245 These data confirm Hha repression of the T3SS in EHEC str. Sakai and TUV93-0, and that
246 HnrS increases expression of T3S proteins in these strains, consistent with anti-silencing of the
247 LEE through *hha* repression.
248
249 **HnrS increases pedestal formation on epithelial cells**
250 Our results suggest that HnrS expression promotes EHEC towards colonisation through
251 decreased motility and increased T3S-mediated attachment. To assess the impact of HnrS and
252 *hha* on host cell interactions, we incubated the Δ*hha* and HnrS knockdowns strains with
253 embryonic bovine lung (EBLs) epithelial cells, a well-established model for attachment and
254 actin pedestal formation of EHEC (45-48). Despite de-repression of the T3SS that is required
255 for attachment and colonisation, we did not observe a statistically significant difference in total
256 attachment with either the Δ*hha* or *hnrS* knockdown strains in the low T3S secretion strain
257 Sakai backgrounds (**Figure 6A**). We next assessed adhesion of the *hnrS* knockdown in the high
258 secretion strain, TUV93-0. As in Sakai, overall attachment to EBL cells was unchanged
259 (**Figure 6B**), but the *hnrS* knockdown had significantly less actin-rich pedestal formation – a
260 key step in T3S-dependant intimate attachment (**Figure 6C**). Quantification at five hours post-
261 infection showed ~60% of WT TUV93-0 bacteria formed actin-rich pedestals versus ~30% of
262 (≈1.91 -fold decrease, p=0.0079). These data suggest that HnrS increases the rate of intimate
263 attachment in EHEC and is consistent with HnrS priming T3SS expression for attachment and
264 colonisation.
265
266 **HnrS promotes expression of genes involved in anaerobic nitrate/nitrite respiration and**
267 **nitric oxide resistance**
268 Hha-H-NS silences a broad range of virulence genes in *E. coli* and *Salmonella* (17, 18, 37)
269 suggesting that HnrS may counter-silence other genes required for colonisation. To enable
270 complementation and avoid CRISPRi off-target effects, we constructed a triple knockout,

271 Δ*hnrS1* Δ*hnrS2* Δ*hnrS3* (hereafter Δ*hnrS*) in the Shiga-toxigenic strain of EHEC str. Sakai
272 using CRISPR–Cas9-mediated genome editing followed by λ-Red recombineering
273 (CRISPathBrick). Deletion of all three copies of *hnrS* was confirmed by Northern blot analysis
274 (**Figure 7A**). The wild-type, Δ*hnrS*, and complemented strains were grown to mid-log phase
275 in T3S-inducing media (supplemented MEM-HEPES). Importantly, HnrS was pulse expressed
276 for 15 minutes before RNA harvesting to primarily capture mRNAs that are direct targets of
277 HnrS. RNA-seq analysis of the transcriptomes indicated that 24-genes were activated in the
278 Δ*hnrS1-3* strain compared to wild type (fold change >2), and 5 were restored to wild type level
279 in the complemented strain **(Supplementary Figure 5)**. While expression levels were low in
280 wild type, *hha* expression was de-repressed in the Δ*hnrS* strain and restored to wild type levels
281 in the complement, consistent with our RNase E-CLASH data and GFP translational fusions
282 (**Figure 7B**).
283
284 Ontological clustering indicated that genes involved in nitrogen metabolism were significantly
285 regulated by HnrS (**Supplementary Figure 6**), including HnrS activation of the *nirBD,*
286 *nrfABCD*, *napA* and *narGU* operons involved in nitrite and nitrate respiration (**Figure 7C**).
287 The nitric oxide reductase encoded by *hcp* was significantly activated by HnrS in the Δ*hnrS*
288 strain and was the most upregulated after pulse expression of HnrS (**Figure 7C**), indicating
289 that HnrS expression promotes expression of nitrite/nitrate respiration genes and nitric oxide
290 detoxification.
291
292 To identify direct targets of HnrS in our differentially expressed genes, we predicted base-
293 pairing complementarity with HnrS and constructed GFP translational fusions for several
294 differentially expressed genes (**Supplementary Figure 7**). Among the nitrogen metabolism
295 genes with complementarity (*nirB*, *nirD*, *hcp*, *nrfA*, *napF*, *narQ*), none were significantly
296 upregulated by HnrS, suggesting that regulation of nitrogen metabolism is indirect.
297
298 To understand how much of this regulation can be explained by HnrS regulation of *hha*, we
299 compared the differentially expressed genes to RNA-seq data from EHEC Δ*hha* (43). Hha
300 regulates a large proportion of the EHEC genome and a substantial subset of genes that were
301 differentially regulated by *hnrS* deletion or pulse expression were also regulated by Hha,
302 (**Supplementary Figure 8**), including several genes involved in nitrogen metabolism (*nirBC*,
303 *napGHJI*, *napBC*). These data suggest that HnrS may act indirectly (at least partly) to regulate
304 nitrogen metabolism operons through repression of Hha.

305

306 During gastrointestinal colonisation, inflammation drives epithelial responses and nitric oxide
307 is secreted by host macrophages to produce NO, which is rapidly oxidised to nitrite and nitrate;
308 these anions accumulate and function as terminal electron acceptors for anaerobic respiration
309 of *E. coli* (24). By repressing *hha*, HnrS appears to promote expression of many nitrate/nitrite
310 respiration and nitric oxide resistance genes required to prime EHEC for survival in the
311 inflamed gastrointestinal tract, at least partly through counter-silencing of *hha*. Together, the
312 data suggest that HnrS primes EHEC for gastrointestinal colonisation by counter-silencing
313 pedestal formation (T3SS) and anaerobic nitrate/nitrite respiration genes while repressing
314 motility.

315 **DISCUSSION**

316

317 H-NS silencing of foreign DNA serves as a final layer of genome defence and allows the cell
318 to balance protecting the genome with acquisition of new genetic information. H-NS silencing
319 is enhanced at horizontally-acquired virulence genes in *E. coli* and *Salmonella* by the H-NS
320 paralogues Hha and YgdT (17, 18, 49). To overcome silencing, many virulence loci encode
321 transcription factors like Ler, Sly, and VirB, that act narrowly to counter-silence specific
322 virulence genes in response to genetic or environmental signals, allowing the virulence genes
323 to be positively selected (15, 50). Complete de-repression of H-NS is likely to have severe
324 fitness costs and deletion of *hns* in *Salmonella* and *Yersina* is lethal (17, 18, 37, 51). H-NS
325 antagonists like the truncated H-NS paralogue, H-NST, are expressed at low levels to avoid
326 full H-NS de-repression (51, 52). Here we demonstrate that the prophage-encoded sRNA,
327 HnrS, relieves Hha-H-NS silencing of the T3SS in EHEC through direct post-transcriptional
328 repression of Hha by base-pairing at its ribosome binding site. We propose that counter-
329 silencing through Hha, rather than H-NS, allows more specific de-repression of horizontally-
330 acquired virulence genes and avoids fitness costs associated with de-repression of the core H-
331 NS regulon.

332

333 We find that HnrS counter-silencing allows EHEC to form more actin-rich pedestals on
334 cultured epithelial cells suggesting that it primes EHEC for gastrointestinal colonisation. This
335 is consistent with down regulation of motility, upregulation of T3SS, and upregulation of genes
336 required for anaerobic nitrate/nitrite respiration and nitric oxide resistance. During mucosal
337 inflammation, epithelial cells and recruited myeloid cells (macrophages and neutrophils)
338 induce inducible nitric oxide synthase (iNOS), generating NO that is rapidly oxidised into
339 nitrates and nitrites (24, 25). These anions accumulate at the hypoxic mucosal surface and
340 function as terminal electron acceptors for anaerobic respiration by *E. coli*. These electrons
341 receptors are used for anaerobic respiration as demonstrated by attenuation of a *napG* mutant
342 encoding nitrate reductase (24, 25). Deletion of *hnrS* reduced expression of several pathways
343 for nitrate and nitrite respiration including *napG* and the NO-detox system *hcp/hcr*. In EHEC,
344 nitrates also trigger maturation of the T3SS by acting as a checkpoint between the basal body
345 and needle filament assembly (24) providing an additional layer of coordination between T3SS
346 and gastrointestinal colonisation. Because HnrS does not directly regulated reporters for
347 several nitrogen metabolism genes, their regulation is likely indirect and *hha*-dependant,
348 although we cannot rule out direct regulation through an untested pathway. Interestingly, *hcp*

349 is strongly upregulated after 15 minutes of HnrS transcription suggesting direct regulation.
350 Collectively, our data indicate that HnrS primes a programme required for gastrointestinal
351 colonisation through counter-silencing of Hha, shifting from a motile/dispersal state towards
352 an attached, pedestal forming, and nitrate-respiring state.
353
354 The HnrS sRNA is encoded on prophages and this has led to repeated acquisition of the sRNA.
355 Both EHEC strains Sakai and EDL933 carry three copies on separate prophage. In some EHEC
356 and EPEC strains *hnrS* has been acquired up to nine times. Additional copies of *hnrS* likely
357 increase expression through gene dosage and we predict that those strains with high copy
358 numbers are likely to have higher levels of counter-silencing. Interestingly, despite being
359 encoded on a mobile genetic element, *hnrS* is almost exclusively found in LEE+ *E. coli* strains,
360 further supporting a function for HnrS in attaching and effacing lesion formation.
361
362 While we have demonstrated that HnrS modulates EHEC virulence gene expression it is less
363 clear whether HnrS provides a selective advantage to the phage. HnrS interacts with the toxin-
364 antitoxin (TA) system *mazEF* in our *in vivo* sRNA interactome data and *in vitro* by EMSA, but
365 we were unable to define a phenotype for this interaction. Several TA systems confer phage
366 resistance through an abortive infection mechanism (53) and MazEF is reported to confer
367 resistance to phages P1 and T4 (34, 35), but we were unable to reproduce this phenotype, or
368 demonstrate HnrS regulation of MazF toxicity or *mazG* expression. A recent study has
369 indicated that MazEF confers resistance to RNA phages (54). Unexpected new functions for
370 sRNAs in regulating co-translational protein folding through interactions with the mRNA
371 coding sequence have recently been uncovered (36). Given the unusual position of the HnrS-
372 *mazF* interaction (perfect complementary to the last 15-nt of the *mazF* coding sequence), we
373 speculate that HnrS may be functioning by a non-canonical mechanism that is not captured by
374 our assays.
375
376 Prophages form one of major building blocks of pathogen evolution and overcoming xenogenic
377 silencing is required for expression and positive selection of virulence genes encoded by the
378 phage. Several mobile elements carry truncated, dominant negative paralogues of H-NS to
379 relieve silencing (16, 52). Here, we find that prophage utilise a regulatory sRNA that counters
380 Hha silencing. HnrS confers Hha-specific counter silencing that likely avoids disrupting the
381 core H-NS regulon. Regulatory sRNAs are compact and highly portable. We predict other

382 mobile genetic elements will encode sRNAs that relieve xenogenic silencing to positively
383 select their virulence gene cargo.
384
385 **METHODS**
386
387 **Bacterial strains and growth conditions**
388
389 Bacterial strains, primers, plasmids and probes used for this study are listed in Supplementary
390 Table 1. *E. coli* was routinely cultured at either 30°C or 37°C in LB broth, minimal M9 broth,
391 MEM-HEPES (Sigma M7278) supplemented with 0.1% glucose and 250 nM $Fe(NO_3)_3$, or
392 solid LB agar plates. Bacterial media was supplemented with ampicillin (100 µg/mL),
393 chloramphenicol (34 µg/mL), kanamycin (50 µg/mL), tetracycline (10 µg/mL) or
394 spectinomycin (50 µg/mL) where appropriate.
395
396 **Construction of EHEC deletion strains**

397 Chromosomal deletions of *hha* and *mazEFG* were constructed using the pTOF25 allelic
398 exchange system (55). Deletion fragments were generated by SOE-PCR and cloned into
399 pTOF25 carrying an FRT–tetRA–FRT cassette for selection. Recombinants were isolated
400 following allelic exchange, confirmed by PCR and sequencing, and the resistance cassette was
401 excised using FLP recombinase (Supplementary Methods).

402 **CRISPRi knockdown of sRNA HnrS**

403 The pCRISPathBrick (pCPB) vector (Addgene, USA) was used for targeted knockdown of
404 *hnrS* in *E. coli* Sakai. sgRNAs targeting *hnrS* were designed, phosphorylated, and annealed.
405 The pCPB vector and sgRNA inserts were digested with BsaI and ligated to generate
406 pCPB::HnrS. The verified plasmid was electroporated into *E. coli* Sakai stx(-) and selected on
407 LB agar with kanamycin and chloramphenicol.

408 **Construction of HnrS deletion in EHEC str. Sakai using CRISPR-Cas9**

409 The HnrS gene in *E. coli* O157:H7 strain Sakai stx^+ was deleted using a CRISPR-Cas9-based
410 system, following a two-plasmid approach (56). The *hnrS* gene in *E. coli* O157:H7 Sakai stx^+
411 was deleted using a CRISPR-Cas9 system with a two-plasmid approach (57). A single guide

412 RNA (sgRNA) targeting *hnrS* was cloned into pTarget-F. Homology arms (~300 bp upstream
413 and downstream of *hnrS*) were joined via SOE PCR and inserted into the pTarget-F vector to
414 generate pTargetT::*hnrS*. Plasmids were transformed into DH5α for propagation and sequence
415 verification. For genome editing, pCas expressing the λ-Red recombination system was
416 introduced into Sakai stx^+, induced with L-arabinose at mid-exponential phase, and
417 pTargetT::*hnrS* was electroporated. Transformants were selected on LB agar with kanamycin
418 and spectinomycin, and deletion of *hnrS* was confirmed by colony PCR. Positive colonies were
419 cured of the editing plasmid by growth on LB-kanamycin with IPTG at 42°C.

420 **Phage plaquing assay**

421 Plaque formation and phage titres were determined using the double-agar overlay method (58,
422 59). LB bottom agar (2% agar) was poured into 10 × 10 cm plates and allowed to dry. Top agar
423 (0.5% agar) was supplemented with 10 mM $CaCl_2$, 10 mM $MgSO_4$, and 800 µL of overnight
424 *E. coli* MG1655 cultures (with or without EcOnc10); for Stx phage assays, 1.5 µg/mL
425 mitomycin C was included. Serial dilutions of phages were spot-plated on the top agar, and
426 plates were incubated overnight at 37°C. Plaques were counted the following day to determine
427 phage titres.

428 **Confirmation of sRNA-mRNA interactions using the sfGFP 2-plasmid system**

429 Prediction of RNA-RNA interaction was done using computational tool IntaRNA (60). GFP
430 translational fusions were generated following established protocols (61, 62). Detailed cloning
431 procedures, including primer sequences and amplification conditions, are provided in
432 Supplementary Methods. In brief, pXG30::*insert* or pXG10::*insert* were co-transformed with
433 either pZE12::*hnrS* or pJV300 (pZE12 encoding a scrambled RNA sequence) into E. coli
434 DH5α. Biological triplicates were grown overnight in LB supplemented with chloramphenicol
435 and ampicillin, overnight cultures were diluted into 15 mL of filtered LB broth supplemented
436 with chloramphenicol and ampicillin, and incubated until OD_{600} reached 0.6. The GFP
437 fluorescence of GFP fusion plasmids was assessed using a POLARstar Omega microplate
438 reader. Fluorescence measurements were taken at an emission wavelength of 510 nm, with an
439 excitation wavelength of 485 nm, which is optimal for GFP fluorescence.

440 **Northern Blot**

441 Total RNA was extracted from *E. coli* O157:H7 str. Sakai using a guanidinium thiocyanate–
442 phenol method (63) (see Supplementary Methods for details). Five micrograms of RNA were
443 separated on 8% denaturing polyacrylamide gels and transferred to nylon membranes. RNA
444 was immobilised by UV-crosslinking, and specific sRNAs were detected using ^{32}P-labelled
445 oligonucleotide probes. Hybridisation and washes were performed under standard conditions,
446 and signals were visualised using a phosphorimager (Typhoon™ FLA9500). Detailed
447 protocols are provided in the Supplementary Methods.

448 **RNA sequencing analysis for gene expression**

449 *E. coli* str. Sakai and isogenic strains grown in MEM-HEPES (Sigma M7278) supplemented
450 with 0.1% glucose and 250 nM $Fe(NO_3)_3$ at 37°C with shaking until OD_{600} 0.8 and RNA
451 extraction was performed as above. Following RNA extraction, samples were treated with RQ1
452 RNase-Free DNase (Promega, Cat. no.: M6101) in the presence of RNasin Ribonuclease
453 inhibitor (Promega, Cat. no.: N2511) for 30 minutes at 37 °C to remove residual genomic DNA.
454 RNA was then purified and concentrated using the Zymo RNA Clean & Concentrator kit
455 (Zymo, Cat. no.: R1019), and quality and concentration were assessed using a Nanodrop
456 spectrophotometer and an Agilent TapeStation 4150 to determine RINe values.

457 The prepared RNA samples were sent to NovogeneAIT Genomics, Singapore for paired-end
458 150 bp sequencing using the NovaSeq platform. Sequencing reads were processed with the
459 READemption v2.0.4 pipeline, aligning reads to the *E. coli* O157:H7 Sakai reference genome
460 (accession number NC_002695.2) and quantifying transcript abundance. Differential gene
461 expression analysis was carried out with a minimum Phred quality score of 30 to ensure high-
462 confidence data. RNA sequencing datasets are available at NCBI GEO under the accession
463 GSE311113.

464 **HnrS prevalence analysis in *E. coli* genomes**

465

466 Genomic data for 3,230 *E. coli* strains were retrieved from NCBI and analysed to assess strain
467 identity, serotype, and pathovar classification. Key housekeeping genes (*recA*, *purA*, *mdh*, *icd*,
468 *gyrB*, *fumC*, *adk*) and virulence/pathotyping markers were identified using K-mer Analysis
469 (KMA) and Shigella/ ST(E)C Finder tools. Boolean logic rules were applied to classify strains
470 into pathovars such as EHEC, EPEC, EAEC, UPEC, and others. The relative coverage of the
471 HnrS was calculated from KMA output by normalising its depth to housekeeping genes,

472 providing an estimate of gene copy number across strains. Detailed methods are provided in
473 Supplementary Methods.

474 **Determination of bacterial motility**

475 Bacterial strains were grown on LB-agar plates and single colonies were subcultured in LB
476 broth to mid-exponential phase. Motility was initially assessed on low-agar plates (0.2% agar)
477 by measuring the diameter of bacterial flares. For single-cell analyses, cultures were diluted to
478 approximately 1×10^5 cells/mL and introduced into flow cells for imaging (64). Bacterial
479 movement was recorded using phase-contrast microscopy with a 40× objective, capturing 20-
480 second time-lapse videos at 20 frames per second. Swimming speeds were determined using
481 custom LabVIEW software(65) and the resulting data were plotted and analysed using
482 GraphPad Prism 8.

483 **Type III secretion assay and immunoblotting**

484 Overnight LB cultures were diluted 1:100 into MEM–HEPES with 250 nM $Fe(NO_3)_3$ and 0.1%
485 glucose and grown to $OD_{600} \approx 0.8$. Cultures were centrifuged, and supernatants were filtered
486 (0.45 µm) and precipitated overnight at 4°C with 10% TCA, using recombinant albumin as a
487 co-precipitant (66). Pellets were resuspended in SDS-PAGE buffer, heated, and separated on
488 4–20% gradient gels, which were stained with Coomassie and imaged.

489 For immunoblotting, proteins were transferred to nitrocellulose, blocked with 8% milk in PBS,
490 and EspD was detected using mouse anti-EspD and HRP-conjugated secondary antibodies with
491 ECL. DnaK in whole-cell lysates was used as a loading control under the same conditions.

492 **Cell adhesion assay**

493 Bovine embryonic lung epithelial cells (EBLs) were seeded at ~10^5 cells/well in 24-well plates
494 and incubated overnight at 37°C with 5% CO_2. Bacterial strains grown overnight in LB were
495 subcultured 1:10 in MEM–HEPES with 0.1% glucose and 250 nM $FeNO_3$ for ~3 h. One hour
496 before infection, EBL media was replaced with MEM–HEPES, and cells were infected at an
497 MOI of ~100. At 3 and 5 h post-infection, wells were washed, and adhered bacteria were
498 recovered by trypsin and quantified by serial dilution plating on LB agar.

499 For microscopy, collagen-coated coverslips were fixed with 1% paraformaldehyde for 10 min,
500 permeabilised with 0.1% Triton X-100 for 10 min and blocked with 1 mg/mL bovine serum
501 albumin for 1 h at room temperature. Cells were incubated with rabbit anti-O157 primary
502 antibody (1:50) for 1 h, followed by Alexa Fluor 568–conjugated goat anti-rabbit IgG
503 secondary antibody (1:1000) for 1 h in the dark. Actin filaments were labelled with Phalloidin–
504 Alexa Fluor 488 (BioLegend) for 30 min, and nuclei were counterstained with Hoechst 33342
505 (1:2000) for 5–10 min. Coverslips were mounted in ProLong Antifade and imaged on a Zeiss
506 LSM900 confocal microscope (63× oil objective) using 488, 568, and 405 nm excitation.
507 Detailed staining procedures are provided in the Supplementary Methods.

508 **Data availability**

509 RNA sequencing datasets generated in this study are available at NCBI GEO under the
510 accession GSE311113.

511

512 **REFERENCES**

513 1. Millman A, Melamed S, Amitai G, Sorek R. 2020. Diversity and classification of cyclic-
514 oligonucleotide-based anti-phage signalling systems. Nature Microbiology 5:1608-
515 1615.
516 2. Navarre WW, McClelland M, Libby SJ, Fang FC. 2007. Silencing of xenogenic DNA
517 by H-NS—facilitation of lateral gene transfer in bacteria by a defense system that
518 recognizes foreign DNA. Genes & Development 21:1456-1471.
519 3. Bustamante VcH, Santana FJ, Calva E, Puente JL. 2001. Transcriptional regulation of
520 type III secretion genes in enteropathogenic *Escherichia coli*: Ler antagonizes H-NS-
521 dependent repression. Molecular Microbiology 39:664-678.
522 4. Corbett D, Bennett HJ, Askar H, Green J, Roberts IS. 2007. SlyA and H-NS regulate
523 transcription of the *Escherichia coli* K5 capsule gene cluster, and expression of *slyA* in
524 *Escherichia coli* is temperature-dependent, positively autoregulated, and independent
525 of H-NS. J Biol Chem 282:33326-33335.
526 5. Haack KR, Robinson CL, Miller KJ, Fowlkes JW, Mellies JL. 2003. Interaction of Ler
527 at the LEE5 (tir) operon of enteropathogenic *Escherichia coli*. Infect Immun 71:384-
528 92.
529 6. Laaberki MH, Janabi N, Oswald E, Repoila F. 2006. Concert of regulators to switch on
530 LEE expression in enterohemorrhagic *Escherichia coli* O157:H7: interplay between
531 Ler, GrlA, HNS and RpoS. Int J Med Microbiol 296:197-210.
532 7. Müller CM, Dobrindt U, Nagy G, Emödy L, Uhlin BE, Hacker J. 2006. Role of histone-
533 like proteins H-NS and StpA in expression of virulence determinants of uropathogenic
534 *Escherichia coli*. J Bacteriol 188:5428-38.
535 8. Torres AG, López-Sánchez GN, Milflores-Flores L, Patel SD, Rojas-López M,
536 Martínez de la Peña CF, Arenas-Hernández MM, Martínez-Laguna Y. 2007. Ler and H-
537 NS, regulators controlling expression of the long polar fimbriae of *Escherichia coli*
538 O157:H7. J Bacteriol 189:5916-28.
539 9. Duan B, Ding P, Navarre WW, Liu J, Xia B. 2021. Xenogenic Silencing and Bacterial
540 Genome Evolution: Mechanisms for DNA Recognition Imply Multifaceted Roles of
541 Xenogenic Silencers. Mol Biol Evol 38:4135-4148.
542 10. Ali SS, Xia B, Liu J, Navarre WW. 2012. Silencing of foreign DNA in bacteria. Current
543 Opinion in Microbiology 15:175-181.
544 11. Doyle M, Fookes M, Ivens A, Mangan MW, Wain J, Dorman CJ. 2007. An H-NS-like
545 stealth protein aids horizontal DNA transmission in bacteria. Science 315:251-2.
546 12. Ellison DW, Young B, Nelson K, Miller VL. 2003. YmoA negatively regulates
547 expression of invasin from *Yersinia enterocolitica*. J Bacteriol 185:7153-9.
548 13. Heroven AK, Nagel G, Tran HJ, Parr S, Dersch P. 2004. RovA is autoregulated and
549 antagonizes H-NS-mediated silencing of invasin and rovA expression in *Yersinia*
550 *pseudotuberculosis*. Mol Microbiol 53:871-88.
551 14. Navarre WW, Porwollik S, Wang Y, McClelland M, Rosen H, Libby SJ, Fang FC. 2006.
552 Selective silencing of foreign DNA with low GC content by the H-NS protein in
553 *Salmonella*. Science 313:236-8.
554 15. Stoebel DM, Free A, Dorman CJ. 2008. Anti-silencing: overcoming H-NS-mediated
555 repression of transcription in Gram-negative enteric bacteria. Microbiology (Reading)
556 154:2533-2545.
557 16. Liu Q, Richardson CC. 1993. Gene 5.5 protein of bacteriophage T7 inhibits the nucleoid
558 protein H-NS of *Escherichia coli*. Proceedings of the National Academy of Sciences
559 90:1761-1765.

17. Aznar S, Paytubi S, Juárez A. 2013. The Hha protein facilitates incorporation of horizontally acquired DNA in enteric bacteria. Microbiology (Reading) 159:545-554.
18. Ali SS, Whitney JC, Stevenson J, Robinson H, Howell PL, Navarre WW. 2013. Structural insights into the regulation of foreign genes in *Salmonella* by the Hha/H-NS complex. J Biol Chem 288:13356-69.
19. Perna NT, Plunkett III G, Burland V, Mau B, Glasner JD, Rose DJ, Mayhew GF, Evans PS, Gregor J, Kirkpatrick HA. 2001. Genome sequence of enterohaemorrhagic *Escherichia coli* O157: H7. Nature 409:529-533.
20. Hayashi T, Makino K, Ohnishi M, Kurokawa K, Ishii K, Yokoyama K, Han CG, Ohtsubo E, Nakayama K, Murata T, Tanaka M, Tobe T, Iida T, Takami H, Honda T, Sasakawa C, Ogasawara N, Yasunaga T, Kuhara S, Shiba T, Hattori M, Shinagawa H. 2001. Complete genome sequence of enterohemorrhagic *Escherichia coli* O157:H7 and genomic comparison with a laboratory strain K-12. DNA Res 8:11-22.
21. Tree JJ, Granneman S, McAteer SP, Tollervey D, Gally DL. 2014. Identification of bacteriophage-encoded anti-sRNAs in pathogenic *Escherichia coli.* Mol Cell 55:199-213.
22. Waters SA, McAteer SP, Kudla G, Pang I, Deshpande NP, Amos TG, Leong KW, Wilkins MR, Strugnell R, Gally DL, Tollervey D, Tree JJ. 2017. Small RNA interactome of pathogenic *E. coli* revealed through crosslinking of RNase E. Embo j 36:374-387.
23. Sy BM, Lan R, Tree JJ. 2020. Early termination of the Shiga toxin transcript generates a regulatory small RNA. Proc Natl Acad Sci U S A 117:25055-25065.
24. Winter SE, Winter MG, Xavier MN, Thiennimitr P, Poon V, Keestra AM, Laughlin RC, Gomez G, Wu J, Lawhon SD, Popova IE, Parikh SJ, Adams LG, Tsolis RM, Stewart VJ, Bäumler AJ. 2013. Host-derived nitrate boosts growth of *E. coli* in the inflamed gut. Science 339:708-11.
25. Nada R, Ebihara S, Yen H, Tobe T. 2020. Enterohaemorrhagic *Escherichia coli* activates nitrate respiration to benefit from the inflammatory response for initiation of microcolony-formation. BMC Microbiol 20:261.
26. Brosse A, Boudry P, Walburger A, Magalon A, Guillier M. 2022. Synthesis of the NarP response regulator of nitrate respiration in *Escherichia coli* is regulated at multiple levels by Hfq and small RNAs. Nucleic Acids Res 50:6753-6768.
27. Waters SA, McAteer SP, Kudla G, Pang I, Deshpande NP, Amos TG, Leong KW, Wilkins MR, Strugnell R, Gally DL, Tollervey D, Tree JJ. 2017. Small RNA interactome of pathogenic *E. coli* revealed through crosslinking of RNase E. The EMBO Journal 36:374-387-387.
28. Sy BM, Lan R, Tree JJ. 2020. Early termination of the Shiga toxin transcript generates a regulatory small RNA. Proceedings of the National Academy of Sciences 117:25055-25065.
29. Zhang X, Payne M, Nguyen T, Kaur S, Lan R. 2021. Cluster-specific gene markers enhance Shigella and enteroinvasive *Escherichia coli* in silico serotyping. Microb Genom 7.
30. Zhang X, Payne M, Kaur S, Lan R. 2021. Improved Genomic Identification, Clustering, and Serotyping of Shiga Toxin-Producing *Escherichia coli* Using Cluster/Serotype-Specific Gene Markers. Front Cell Infect Microbiol 11:772574.
31. Chase-Topping M, Dallman TJ, Allison L, Lupolova N, Matthews L, Mitchell S, Banks CJ, Prentice J, Brown H, Tongue S, Henry M, Evans J, Gunn G, Hoyle D, McNeilly TN, Fitzgerald S, Smith-Palmer A, Shaaban S, Holmes A, Hanson M, Woolhouse M, Didelot X, Jenkins C, Gally DL. 2023. Analysis of *Escherichia coli* O157 strains in

609 cattle and humans between Scotland and England & Wales: implications for human
610 health. Microb Genom 9.
611 32. Sprenger M, Siemers M, Krautwurst S, Papenfort K. 2024. Small RNAs direct attack
612 and defense mechanisms in a quorum sensing phage and its host. Cell Host & Microbe
613 32:727-738.e6.
614 33. Silverman A, Nashef R, Bruner R, Noy T, Melamed S. 2024. Phage-encoded small RNA
615 hijacks host replication machinery to support the phage lytic cycle. bioRxiv
616 doi:10.1101/2024.10.31.621285:2024.10.31.621285.
617 34. Alawneh AM, Qi D, Yonesaki T, Otsuka Y. 2016. An ADP-ribosyltransferase Alt of
618 bacteriophage T4 negatively regulates the *Escherichia coli* MazF toxin of a toxin-
619 antitoxin module. Mol Microbiol 99:188-98.
620 35. Hazan R, Engelberg-Kulka H. 2004. *Escherichia coli mazEF*-mediated cell death as a
621 defense mechanism that inhibits the spread of phage P1. Mol Genet Genomics 272:227-
622 34.
623 36. Thongdee N, Alaniz MM, Samatova E, Zhong A, Esnault C, Zhang H, Dale RK,
624 Rodnina MV, Storz G. 2025. Modulation of protein activity by small RNA base pairing
625 internal to coding sequences. Molecular Cell 85:1824-1837.e7.
626 37. Bae S-H, Liu D, Lim HM, Lee Y, Choi B-S. 2008. Structure of the Nucleoid-Associated
627 Protein Cnu Reveals Common Binding Sites for H-NS in Cnu and Hha. Biochemistry
628 47:1993-2001.
629 38. Sharma VK, Casey TA. 2014. Determining the relative contribution and hierarchy of
630 *hha* and *qseBC* in the regulation of flagellar motility of *Escherichia coli* O157:H7.
631 PLoS One 9:e85866.
632 39. Sharma VK, Bearson BL. 2013. Hha controls *Escherichia coli* O157:H7 biofilm
633 formation by differential regulation of global transcriptional regulators FlhDC and
634 CsgD. Appl Environ Microbiol 79:2384-96.
635 40. Sharma VK, Carlson SA, Casey TA. 2005. Hyperadherence of an *hha* mutant of
636 *Escherichia coli* O157:H7 is correlated with enhanced expression of LEE-encoded
637 adherence genes. FEMS Microbiol Lett 243:189-96.
638 41. Sharma VK, Zuerner RL. 2004. Role of *hha* and *ler* in transcriptional regulation of the
639 *esp* operon of enterohemorrhagic *Escherichia coli* O157:H7. J Bacteriol 186:7290-301.
640 42. Fukui N, Oshima T, Ueda T, Ogasawara N, Tobe T. 2016. Gene Activation through the
641 Modulation of Nucleoid Structures by a Horizontally Transferred Regulator, Pch, in
642 Enterohemorrhagic *Escherichia coli*. PLoS One 11:e0149718.
643 43. Paytubi S, Dietrich M, Queiroz MH, Juárez A. 2013. Role of plasmid- and
644 chromosomally encoded Hha proteins in modulation of gene expression in *E. coli*
645 O157:H7. Plasmid 70:52-60.
646 44. Sharma VK, Sacco RE, Kunkle RA, Bearson SM, Palmquist DE. 2012. Correlating
647 levels of type III secretion and secreted proteins with fecal shedding of *Escherichia coli*
648 O157:H7 in cattle. Infect Immun 80:1333-42.
649 45. Tree JJ, Roe AJ, Flockhart A, McAteer SP, Xu X, Shaw D, Mahajan A, Beatson SA,
650 Best A, Lotz S, Woodward MJ, La Ragione R, Murphy KC, Leong JM, Gally DL. 2011.
651 Transcriptional regulators of the GAD acid stress island are carried by effector protein-
652 encoding prophages and indirectly control type III secretion in enterohemorrhagic
653 *Escherichia coli* O157:H7. Mol Microbiol 80:1349-65.
654 46. Bai J, McAteer SP, Paxton E, Mahajan A, Gally DL, Tree JJ. 2011. Screening of an E.
655 coli O157:H7 Bacterial Artificial Chromosome Library by Comparative Genomic
656 Hybridization to Identify Genomic Regions Contributing to Growth in Bovine
657 Gastrointestinal Mucus and Epithelial Cell Colonization. Front Microbiol 2:168.

658 47. Wells TJ, Sherlock O, Rivas L, Mahajan A, Beatson SA, Torpdahl M, Webb RI, Allsopp
659 LP, Gobius KS, Gally DL, Schembri MA. 2008. EhaA is a novel autotransporter protein
660 of enterohemorrhagic *Escherichia coli* O157:H7 that contributes to adhesion and
661 biofilm formation. Environ Microbiol 10:589-604.
662 48. Wolfson EB, Elvidge J, Tahoun A, Gillespie T, Mantell J, McAteer SP, Rossez Y, Paxton
663 E, Lane F, Shaw DJ, Gill AC, Stevens J, Verkade P, Blocker A, Mahajan A, Gally DL.
664 2020. The interaction of *Escherichia coli* O157:H7 and *Salmonella* Typhimurium
665 flagella with host cell membranes and cytoskeletal components. Microbiology
666 (Reading) 166:947-965.
667 49. Ali SS, Soo J, Rao C, Leung AS, Ngai DH, Ensminger AW, Navarre WW. 2014.
668 Silencing by H-NS potentiated the evolution of Salmonella. PLoS Pathog 10:e1004500.
669 50. Colgan AM, Kröger C, Diard M, Hardt WD, Puente JL, Sivasankaran SK, Hokamp K,
670 Hinton JC. 2016. The Impact of 18 Ancestral and Horizontally-Acquired Regulatory
671 Proteins upon the Transcriptome and sRNA Landscape of *Salmonella enterica* serovar
672 Typhimurium. PLoS Genet 12:e1006258.
673 51. Baños RC, Pons JI, Madrid C, Juárez A. 2008. A global modulatory role for the *Yersinia*
674 *enterocolitica* H-NS protein. Microbiology (Reading) 154:1281-1289.
675 52. Williamson HS, Free A. 2005. A truncated H-NS-like protein from enteropathogenic
676 *Escherichia coli* acts as an H-NS antagonist. Mol Microbiol 55:808-27.
677 53. Jurenas D, Fraikin N, Goormaghtigh F, Van Melderen L. 2022. Biology and evolution
678 of bacterial toxin-antitoxin systems. Nat Rev Microbiol doi:10.1038/s41579-021-
679 00661-1.
680 54. Nikolic N, Pleška M, Bergmiller T, Guet CC. 2025. A bacterial toxin-antitoxin system
681 as a native defence element against RNA phages. Biol Lett 21:20250080.
682 55. Merlin C, McAteer S, Masters M. 2002. Tools for characterization of *Escherichia coli*
683 genes of unknown function. J Bacteriol 184:4573-81.
684 56. Jiang Y, Chen B, Duan C, Sun B, Yang J, Yang S. 2015. Multigene editing in the
685 *Escherichia coli* genome via the CRISPR-Cas9 system. Appl Environ Microbiol
686 81:2506-14.
687 57. Yang X, Bai X, Zhang J, Sun H, Fu S, Fan R, He X, Scheutz F, Matussek A, Xiong Y.
688 2020. *Escherichia coli* strains producing a novel Shiga toxin 2 subtype circulate in
689 China. Int J Med Microbiol 310:151377.
690 58. Islam MR, Ogura Y, Asadulghani M, Ooka T, Murase K, Gotoh Y, Hayashi T. 2012. A
691 sensitive and simple plaque formation method for the Stx2 phage of *Escherichia coli*
692 O157:H7, which does not form plaques in the standard plating procedure. Plasmid
693 67:227-35.
694 59. Bonanno L, Loukiadis E, Mariani-Kurkdjian P, Oswald E, Garnier L, Michel V, Auvray
695 F, Griffiths MW. 2015. Diversity of Shiga Toxin-Producing Escherichia coli (STEC)
696 O26:H11 Strains Examined via *stx* Subtypes and Insertion Sites of Stx and EspK
697 Bacteriophages. Applied and Environmental Microbiology 81:3712-3721.
698 60. Mann M, Wright PR, Backofen R. 2017. IntaRNA 2.0: enhanced and customizable
699 prediction of RNA-RNA interactions. Nucleic Acids Res 45:W435-w439.
700 61. Urban JH, Vogel J. 2007. Translational control and target recognition by *Escherichia*
701 *coli* small RNAs in vivo. Nucleic Acids Res 35:1018-37.
702 62. Corcoran CP, Podkaminski D, Papenfort K, Urban JH, Hinton JC, Vogel J. 2012.
703 Superfolder GFP reporters validate diverse new mRNA targets of the classic porin
704 regulator, MicF RNA. Mol Microbiol 84:428-45.
705 63. Tollervey D, Mattaj IW. 1987. Fungal small nuclear ribonucleoproteins share properties
706 with plant and vertebrate U-snRNPs. Embo j 6:469-76.

64. Scadden J, Ridone P, Pandit D, Sowa Y, Baker Matthew AB. 2025. Rescue of bacterial motility using two- and three-species FliC chimeras. Journal of Bacteriology 207:e00517-24.
65. Ishida T, Ito R, Clark J, Matzke NJ, Sowa Y, Baker MAB. 2019. Sodium-powered stators of the bacterial flagellar motor can generate torque in the presence of phenamil with mutations near the peptidoglycan-binding region. Mol Microbiol 111:1689-1699.
66. Roe Andrew J, Yull H, Naylor Stuart W, Woodward Martin J, Smith David GE, Gally David L. 2003. Heterogeneous Surface Expression of EspA Translocon Filaments by *Escherichia coli* O157:H7 Is Controlled at the Posttranscriptional Level. Infection and Immunity 71:5900-5909.

719 **FIGURES LEGENDS**

720

721 **Figure 1. *E. coli* str. Sakai encodes three identical copies of sRNA HnrS on prophage. A.**
722 RNA end mapping, Hfq, and RNase E binding at HnrS. Total RNA-seq data from EHEC grown
723 in MEM-HEPES (purple, [23]), dRNA-seq (light green, TEX-), dRNA-seq dark green, TEX+),
724 and Term-seq (red bar plot), Hfq binding (orange, [21]), and RNase E binding (dark blue, [22])
725 for three genomic copies of HnrS in EHEC str. Sakai. Read abundance is indicated on the y-
726 axis. Term-seq peaks correspond to transcription termination sites, while dRNA-seq reads
727 highlight transcription start sites. Grey arrows indicate the position of HnrS with the systematic
728 name and prophages (Sp9, Sp10, and Sp12) in brackets. **B.** Northern blot analysis of HnrS
729 expression in LB, minimal M9, and MEM-HEPES media at mid-exponential (OD600 = 0.6),
730 late exponential (OD600 = 1.0), and early stationary (OD600 = 1.8) phases.

731

732 **Figure 2. Distribution and coverage of HnrS across *E. coli* pathotypes and serotypes. A.**
733 Coverage of *hnrS* across different *E. coli* pathotypes, including EHEC, EPEC, UPEC, and
734 others where values were normalised to six conserved housekeeping genes (*arpA*, *trpA*, *uidA*,
735 *rrl*, *tspE4*, and *fyuA*) as a reference. **B.** Violin plot representing maximum *hnrS* coverage across
736 EHEC, EPEC and UPEC strains. **C.** Distribution of *hnrS* read coverage across STEC serotypes.
737 Asterisks above the violins indicate statistically significant deviations from the overall median,
738 as determined by one-sample t-tests. **D.** Box plot of *hnrS* coverage (FPKM) in O157:H7
739 isolates from human and cattle sources.

740

741 **Figure 3. *In silico* and experimental validation of HnrS–mRNA interactions. A.** Predicted
742 interactions of HnrS with *hha* and *asnC* mRNAs using IntaRNA. **B.** Target mRNA–sfGFP
743 fluorescence in the presence of HnrS or scrambled control plasmid (pJV300) for the first six
744 genes in the RNA interactome. **C.** Compensatory point mutations (blue) were introduced in
745 *hha* or HnrS at the M1 seed region to disrupt predicted base-pairing. The sequence AGAAG
746 upstream of the *hha* coding region corresponds to the ribosome binding site (RBS). **D.**
747 Fluorescence of *hha*–sfGFP was measured in the presence of HnrS wild type or mutant
748 variants, with restoration of interaction by complementary mutations confirming direct pairing.
749 Data represents mean GFP intensity from three biological replicates with two technical
750 replicates each.

751

752

753

754 **Figure 4. Δ*hha* and HnrS mutants exhibit altered motility. A.** Single-cell swimming speed
755 of EHEC str. Sakai wild type, Δ*hha* with empty vector (pBR322), and Δ*hha* complemented
756 with pBR322::*hha*. Cells were imaged in tunnel slides under phase-contrast microscopy, and
757 20-second videos were captured at 20 frames per second (400 frames total) using a Chameleon3
758 CM3 camera. Speeds <0.5 µm/s were excluded as non-motile. Data were analyzed with
759 LabView and visualised in GraphPad Prism 10 (WT n=118, Δ*hha* n=11, complemented n=30,
760 Mann-Whitney test). **B.** Single-cell speed assay for *E. coli* RP437 wild type, RP437 with empty
761 vector (pJV300), and RP437 carrying pZE12::*hnrS.* **C.** Northern blot detecting HnrS
762 expression in wild type and HnrS CRISPRi knockdown strains (pCPB vector), with RNA
763 harvested at early stationary phase (OD_{600}=1.8). **D.** Single-cell speed assay for EHEC Sakai
764 stx(-) strains with empty vector (pCPB) and EcOnc10 knockdown (pCPB::sgHnrS). Videos
765 were captured and analysed as described in panel A.

766 **Figure 5. T3SS secretion profiles of hha and HnrS mutants in EHEC Sakai and TUV 93-**
767 **0 strains. A.** Coomassie-stained SDS-PAGE gels showing secreted protein profiles. ***Left***
768 ***panel:*** EHEC Sakai stx(-) wild type, wild type with pBR322, Δ*hha*, Δ*hha* with pBR322, and
769 Δ*hha* complemented with pBR322::*hha*. ***Middle panel:*** EHEC TUV 93-0 stx(-) wild type,
770 Δ*hha*, and Δ*hha* complemented with pBR322::*hha.* **B.** Coomassie-stained secreted protein
771 profiles for HnrS knockdown strains. EHEC TUV 93-0 and Sakai strains carrying either the
772 empty vector (pCPB) or pCPB::sgHnrS. Arrows indicate BSA (loading control, 66.4 kDa),
773 EspB/D (needle tip proteins, 32.6 kDa and 39.1 kDa), and EspA (filament, 20.6 kDa). **C.**
774 Western blot analysis of EspD in secreted fractions and DnaK in whole-cell samples. *Top*
775 *panel:* Sakai derivatives, including wild type with pBR322 (lane 1), Δ*hha* with pBR322 (lane
776 2), and Δ*hha* complemented with pBR322::*hha* (lane 3). ***Bottom panel:*** Additional strains,
777 including TUV 93-0 with pCPB (lane 1), TUV 93-0 with pCPB::sgHnrS (lane 2), Sakai with
778 pCPB (lane 3), and Sakai with pCPB::sgHnrS (lane 4). Densitometry analysis of the EspD
779 bands from these blots is shown alongside each Western blot. Chemiluminescence images from
780 a technical replicate were quantified using ImageJ. Statistical significance was assessed by
781 unpaired t-test

782

783 **Figure 6. Immunofluorescence analysis of EBL cells infected with EHEC *hha* and HnrS**
784 **mutants. A. Left panel:** EBLs were infected with EHEC Sakai strains carrying pBR322 (wild
785 type), Δ*hha* with pBR322, and the complemented Δ*hha* strain with pBR322::*hha* (MOI 100).
786 Bacteria including flagella (magenta) were visualized using anti-O157 antibodies with Alexa
787 Fluor 568 secondary, nuclei (yellow) were stained with Hoechst 33342, and actin filaments
788 (cyan) were visualized with Phalloidin-FITC. Merged images show co-localization of all stains.
789 Wild type shows intact flagella, Δ*hha* lacks flagella, and the complemented strain restores
790 flagella expression. **Right panel:** EBLs were infected with EHEC Sakai carrying either pCPB
791 (empty vector) or pCPB::sgHnrS (HnrS knockdown) at MOI 100. **B.** EBLs were infected with
792 EHEC TUV 93-0 carrying either pCPB (empty vector) or pCPB:: sgHnrS (HnrS knockdown)
793 at MOI 100. **C.** The percentage of bacteria inducing actin polymerisation at adhesion sites was
794 measured from fluorescence images. TUV 93-0 EcOnc10 knockdown shows significantly
795 reduced actin polymerization compared to the wild type

796 **Figure 7. HnrS expression and its impact on nitrate and nitrite respiration genes. A.**
797 Northern blot showing HnrS expression in wild type (WT), Δ*hnrS*, and complemented strains
798 with pulse expression from pBAD+1::HnrS. RNA was harvested at mid-exponential (OD_{600} =
799 0.8) and early stationary phase (OD_{600} = 1.8). **B.** Bar graph showing the expression levels of
800 RNase E CLASH targets of HnrS in RNA seq data. Gene expression is quantified by read
801 counts from biological triplicates, based on DESeq data. **C.** Bar graph depicting the expression
802 of genes involved in nitrate and nitrite respiration, showing reduced expression in ΔHnrS
803 relative to WT and complemented strains. Gene expression is quantified from DESeq2 read
804 counts of biological triplicates. *narU.1*, *narG.1*, and *narY.1* correspond to *E. coli* O157:H7
805 Sakai homologues that are not present in *E. coli* K-12 MG1655, although they share
806 nomenclature with *narU*, *narG*, and *narY*.

807

808

809 **SUPPLEMENTARY FIGURES**

810 **Supplementary Figure 1. HnrS is encoded within prophages in E. coli pathotypes.**
811 Prophage regions from eight different E. coli pathotypes were aligned based on sequence
812 similarities between their prophage genomes as determined by BLAST. HnrS is indicated in
813 pink and labelled as EcOnc10 in the alignment. Annotations for phage genes and hypothetical
814 proteins are shown in blue and were retrieved from NCBI; however, no annotations are
815 available for the prophage regions of the EPEC strain E1110019. On the left, the pathotype,
816 serotype, and strain identifiers are listed, followed by either the name of the prophage (for strain
817 Sakai) or the region number assigned by PHASTER. For strain Sakai's prophage Sp9, the
818 regions responsible for phage replication, regulation, lysis, packaging, head, and tail fibre genes
819 are marked.

820 **Supplementary Figure 2: HnrS interaction with the MazEF toxin-antitoxin system and**
821 **phage sensitivity assays. A.** *In silico* prediction of HnrS binding to the *mazF* mRNA, showing
822 the predicted interaction site along with neighbouring genes in the *mazEFG* operon. **B.** EMSA
823 to show HnrS interacts with *mazF* coding sequence invitro. **C.** Top. Plaquing assay to assess
824 the sensitivity of *E. coli* K12 wild type (top) and Δ*mazEFG* (bottom) to a panel of phages,
825 including P1kc, T4-like, λ, and V5. Serial dilutions of each phage were spot plated onto the
826 respective bacterial strains, and phage plaques were counted to assess bacterial sensitivity.
827 Bottom: Sensitivity of EHEC strain Sakai, Sakai Δ*mazEFG*, and complemented strains
828 (overexpressing *mazEFG* from pBR322) to Stx phage induction (bottom).

829 **Supplementary Figure 3: HnrS does not repress MazEF toxicity in *E. coli.* A.** Growth
830 curves of *E. coli* Top10F' overexpressing HnrS (pZE12::HnrS) and/or MazEFG
831 (pZA21::mazEFG) under different induction conditions. Cultures were grown at 37°C with
832 shaking for 24 hours in a Bioscreen C system. Panels show growth without aTc (no MazEFG
833 induction) and with increasing aTc concentrations (0.1, 1, 10, 100 ng/mL) to induce MazEFG
834 expression. Control plasmid combinations are indicated as described in Materials and Methods.
835 **B.** Fluorescence of a MazEFG-sfGFP translational fusion in *E. coli* DH5α under different
836 expression conditions of HnrS. Error bars represent standard deviations from biological
837 replicates.

838 **Supplementary Figure 4. GFP fluorescence versus OD600 for LEE promoter fusions.**
839 Individual LEE operon promoters (*ler* , *tir*, *sepL)* were fused to GFP and introduced into EHEC

840 Sakai strains carrying either pBR322 (wild type), Δhha with pBR322, or Δhha complemented
841 with pBR322::hha. The promoter-less GFP plasmid pAJR70 served as a control. Fluorescence
842 (GFP) and OD600 were recorded every 20 minutes. Data points represent the mean of three
843 biological replicates, each with two technical duplicates; error bars indicate ±1 SD. A
844 representative experiment of at least three independent trials is shown.

845 **Supplementary Figure 5. Differential gene expression analysis of EHEC Sakai strains**
846 **under wild type, deletion, and complementation of HnrS. A:** Volcano plot showing
847 differentially expressed genes between the deletion mutant (EHEC Sakai ΔHnrS) and the wild
848 type (fold change ≥ 2, $p < 0.05$). **B:** Volcano plot comparing the deletion mutant (EHEC Sakai
849 ΔHnrS) to the complementation strain (EHEC Sakai ΔHnrS with pBAD+1::*hnrS*). Green and
850 red dots indicate significantly upregulated and downregulated genes, respectively.

851 **Supplementary Figure 6. Gene Ontology (GO) analysis of differentially expressed genes**
852 **(DEGs) between the ΔHnrS mutant and wild type strain.** GO analysis under the Biological
853 Process category identified processes significantly enriched (p-adjusted < 0.05) in the wild type
854 strain compared to the ΔHnrS mutant.

855 **Supplementary Figure 7. GFP translation fusion assay of genes involved in nitrate**
856 **respiration.** Bar graphs show fluorescence from translation fusions of NirB, NapF, NirD,
857 NrfA, NarQ, and Hcp measured in the presence of HnrS or the control plasmid pJV300. The
858 background control, pXG0, is included to account for autofluorescence, while insert **(-)**
859 represents the empty **pXG10-SF** vector.

860 **Supplementary Figure 8. Comparative regulation of genes by Hha and HnrS.** Scatterplot
861 matrix showing relationships among Δ*hha*/WT and WT/Δ*hnrS*. Each panel represents pairwise
862 comparisons of $\log_2$ fold-change values from RNA-seq experiments. Red points indicate
863 nitrogen metabolism genes, including *nirB, nirC, napG, napH, nrfF, nrfG, narI, narJ, napB,*
864 *napC, glnA, gltB, gltD, ntrC,* and *amtB*, while grey points represent all other genes. Diagonal
865 panels show density distributions of each dataset. Dashed lines indicate zero fold-change, and
866 dotted lines indicate the diagonal (slope = 1) in pairwise scatter plots. Data are corrected such
867 that the direction of regulation is consistent across comparisons (e.g., WT/Δ*hnrS* is inverted
868 relative to Δ*hnrS*/WT).

869

Figure 1

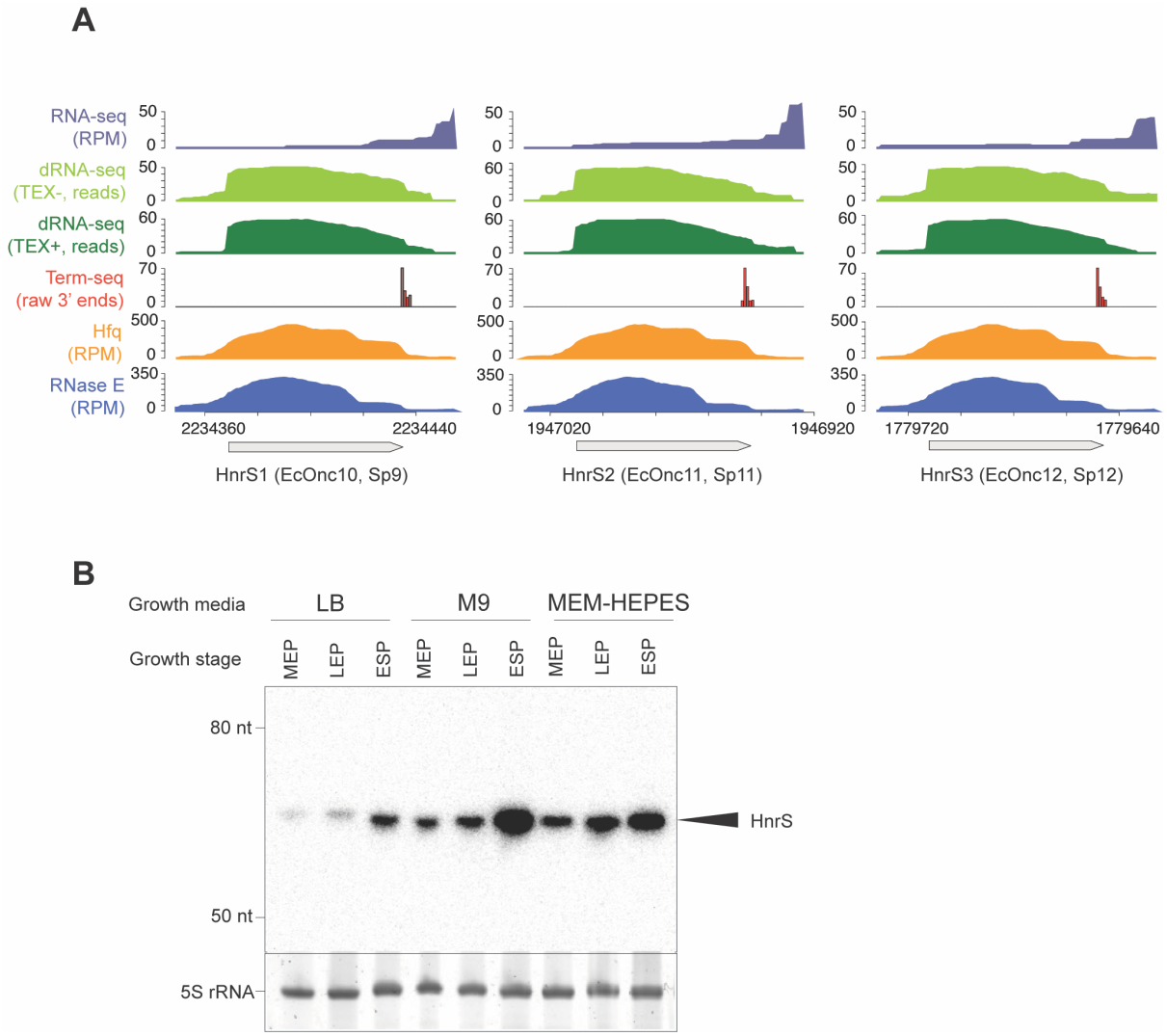
A
RNA-seq (RPM)
dRNA-seq (TEX-, reads)
dRNA-seq (TEX+, reads)
Term-seq (raw 3' ends)
Hfq (RPM)
RNase E (RPM)
2234360
2234440
1947020
1946920
1779720
1779640
HnrS1 (EcOnc10, Sp9)
HnrS2 (EcOnc11, Sp11)
HnrS3 (EcOnc12, Sp12)
B
Growth media
LB
M9
MEM-HEPES
Growth stage
MEP
LEP
ESP
80 nt
50 nt
HnrS
5S rRNA

Figure 2

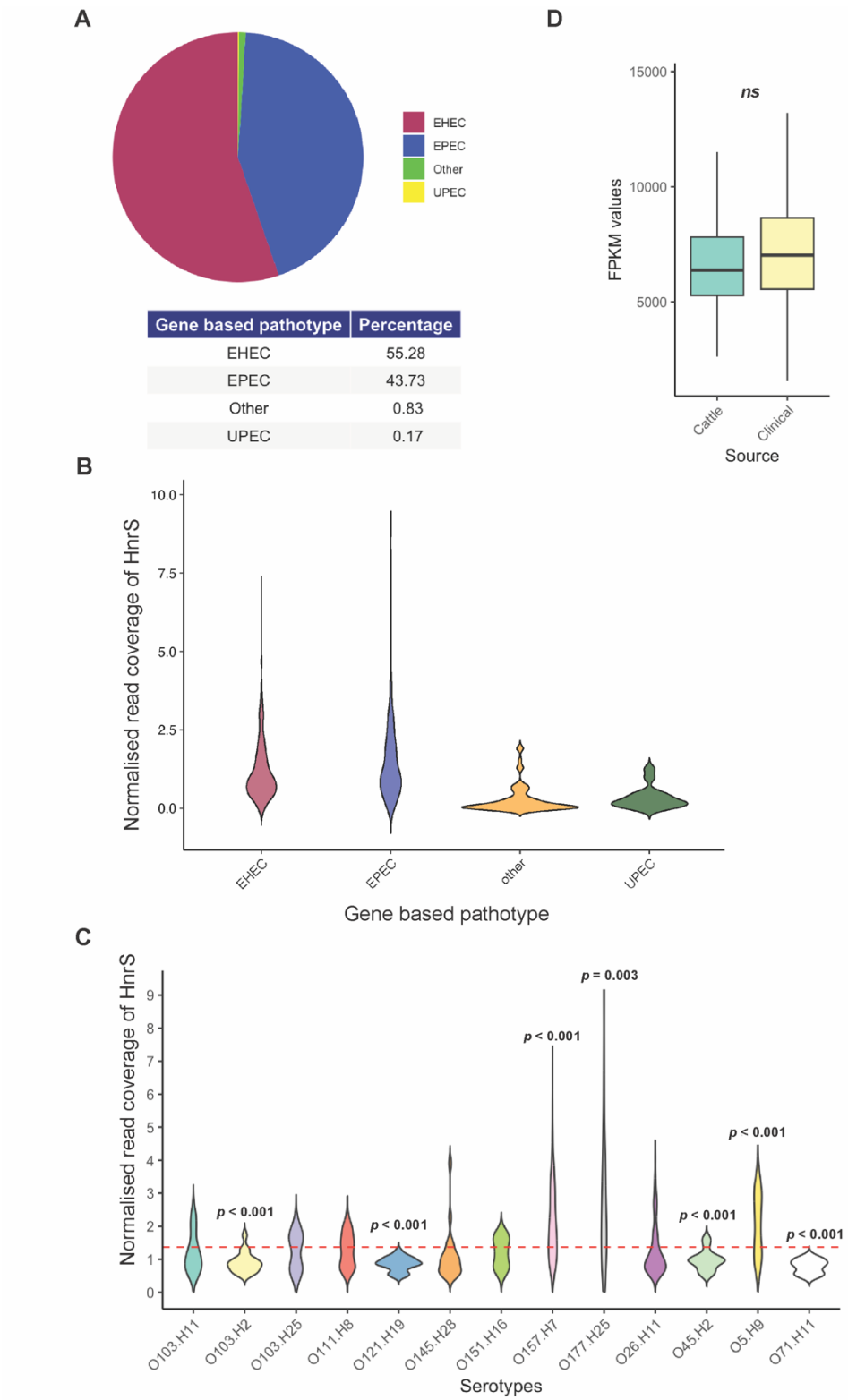

Gene based pathotype	Percentage
EHEC	55.28
EPEC	43.73
Other	0.83
UPEC	0.17

Figure 3

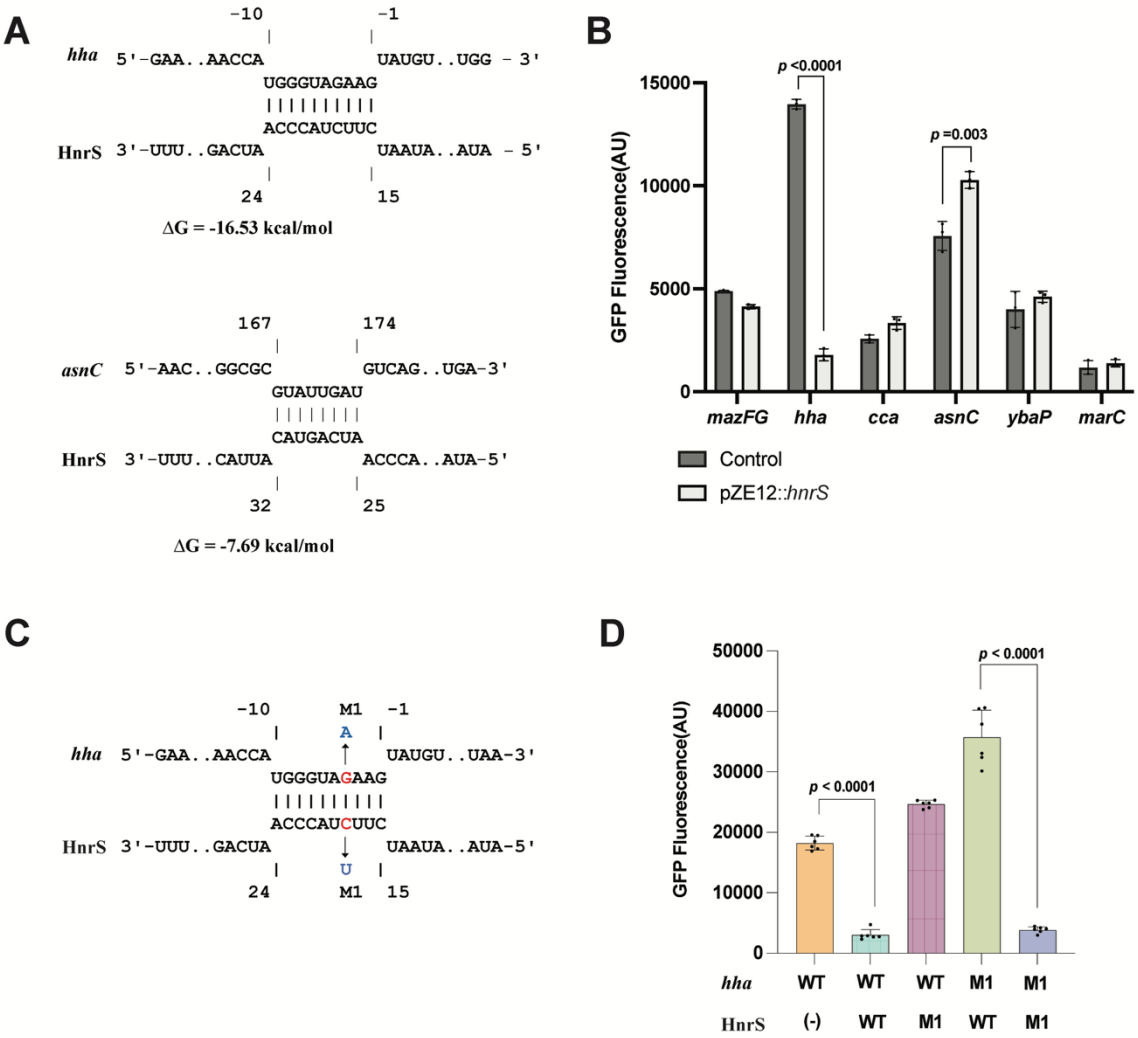
A
-10
-1
hha 5'-GAA..AACCA
UAUGU..UGG - 3'
UGGGUAGAAG
ACCCAUCUUC
HnrS 3'-UUU..GACUA
UAAUA..AUA - 5'
24
15
ΔG = -16.53 kcal/mol
167
174
asnC 5'-AAC..GGCGC
GUCAG..UGA-3'
GUAUUGAU
CAUGACUA
HnrS 3'-UUU..CAUUA
ACCCA..AUA-5'
32
25
ΔG = -7.69 kcal/mol
B
GFP Fluorescence(AU)
15000
10000
5000
0
p <0.0001
p =0.003
mazFG
hha
cca
asnC
ybaP
marC
Control
pZE12::hnrS
C
-10
M1
-1
hha 5'-GAA..AACCA
UAUGU..UAA-3'
UGGGUAGAAG
ACCCAUCUUC
HnrS 3'-UUU..GACUA
UAAUA..AUA-5'
24
M1
15
D
GFP Fluorescence(AU)
50000
40000
30000
20000
10000
0
p < 0.0001
p < 0.0001
hha WT WT WT M1 M1
HnrS (-) WT M1 WT M1

Figure 4

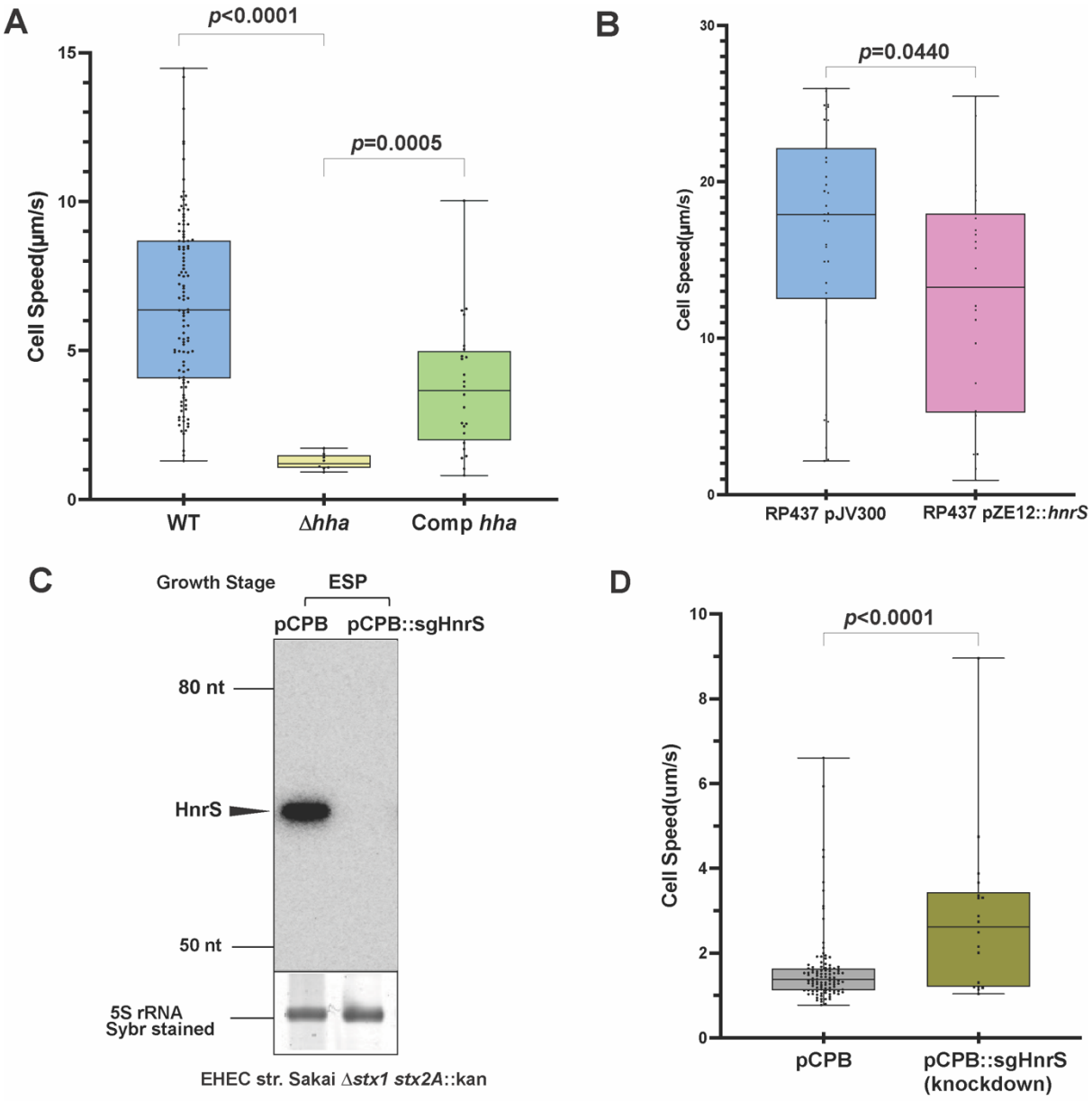
A
p<0.0001
p=0.0005
Cell Speed(µm/s)
15
10
5
0
WT
Δhha
Comp hha
B
p=0.0440
Cell Speed(µm/s)
30
20
10
0
RP437 pJV300
RP437 pZE12::hnrS
C
Growth Stage
ESP
pCPB
pCPB::sgHnrS
80 nt
HnrS
50 nt
5S rRNA
Sybr stained
EHEC str. Sakai Δstx1 stx2A::kan
D
p<0.0001
Cell Speed(um/s)
10
8
6
4
2
0
pCPB
pCPB::sgHnrS
(knockdown)

Figure 5

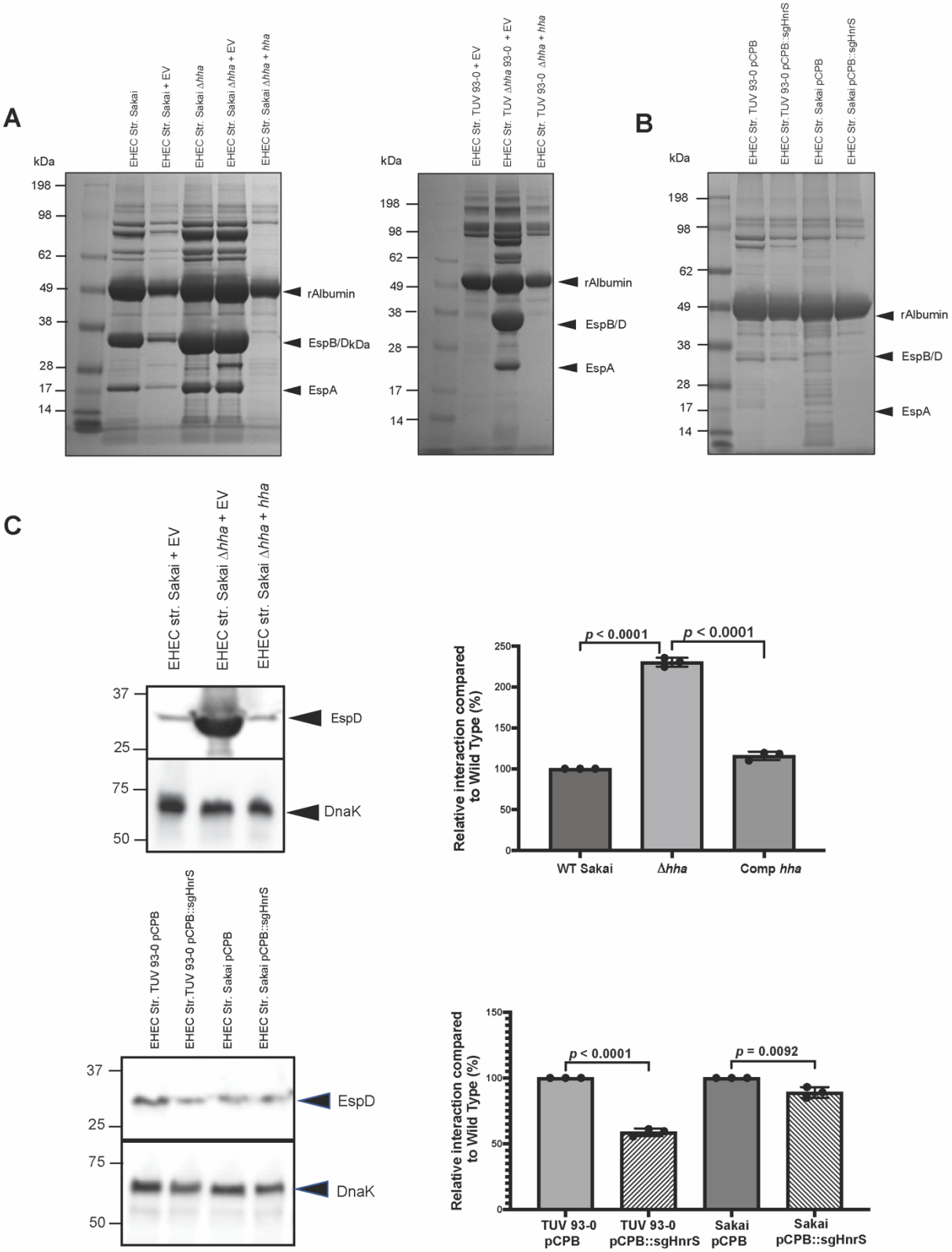
A
kDa
EHEC Str. Sakai
EHEC Str. Sakai + EV
EHEC Str. Sakai Δhha
EHEC Str. Sakai Δhha + EV
EHEC Str. Sakai Δhha + hha
198
98
62
49
38
28
17
14
rAlbumin
EspB/DkDa
EspA
EHEC Str. TUV 93-0 + EV
EHEC Str. TUV Δhha 93-0 + EV
EHEC Str. TUV 93-0 Δhha + hha
EspB/D
B
EHEC Str. TUV 93-0 pCPB
EHEC Str. TUV 93-0 pCPB::sgHnrS
EHEC Str. Sakai pCPB
EHEC Str. Sakai pCPB::sgHnrS
C
EHEC str. Sakai + EV
EHEC str. Sakai Δhha + EV
EHEC str. Sakai Δhha + hha
37
25
75
50
EspD
DnaK
Relative interaction compared to Wild Type (%)
p < 0.0001
p < 0.0001
WT Sakai
Δhha
Comp hha
p = 0.0092
TUV 93-0 pCPB
TUV 93-0 pCPB::sgHnrS
Sakai pCPB
Sakai pCPB::sgHnrS

Figure 6

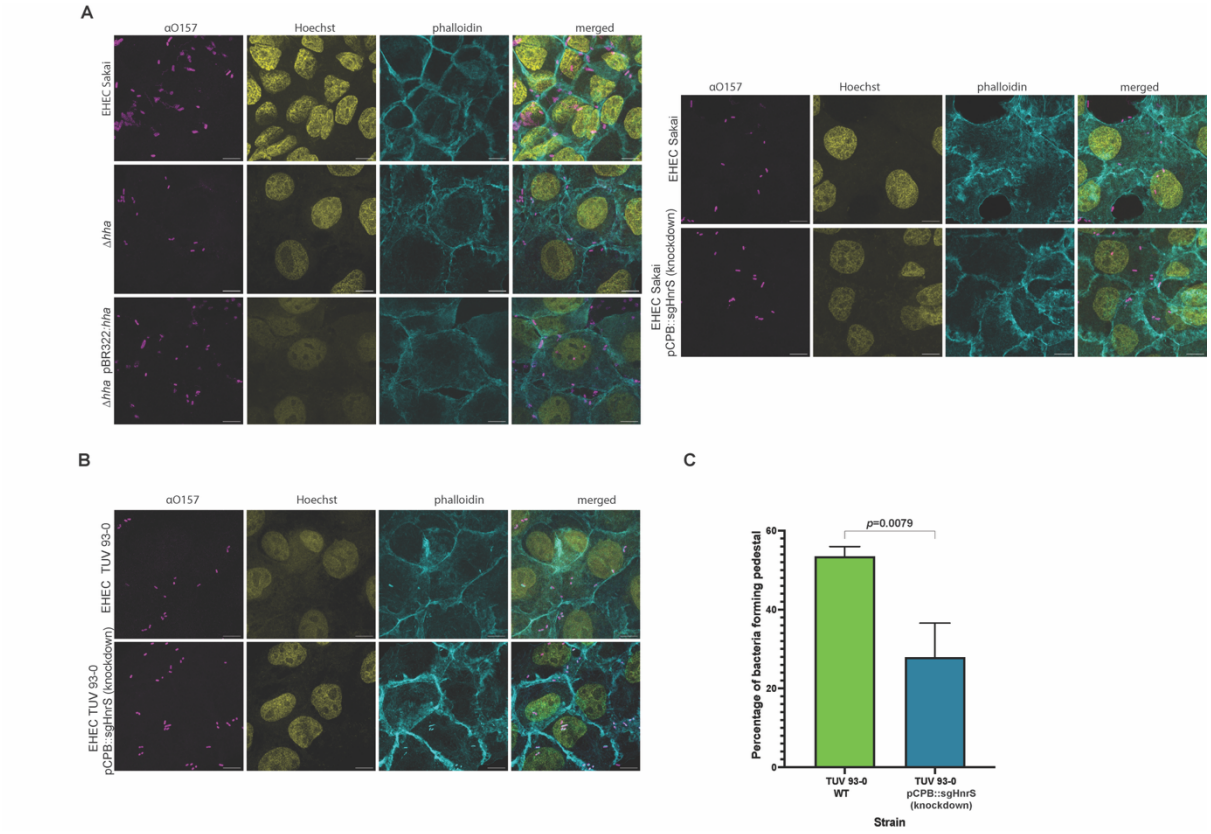
A
αO157
Hoechst
phalloidin
merged
EHEC Sakai
Δhha
Δhha pBR322:hha
EHEC Sakai
EHEC Sakai pCPB::sgHnrS (knockdown)
B
EHEC TUV 93-0
EHEC TUV 93-0 pCPB::sgHnrS (knockdown)
C
p=0.0079
Percentage of bacteria forming pedestal
0
20
40
60
TUV 93-0 WT
TUV 93-0 pCPB::sgHnrS (knockdown)
Strain

Figure 7

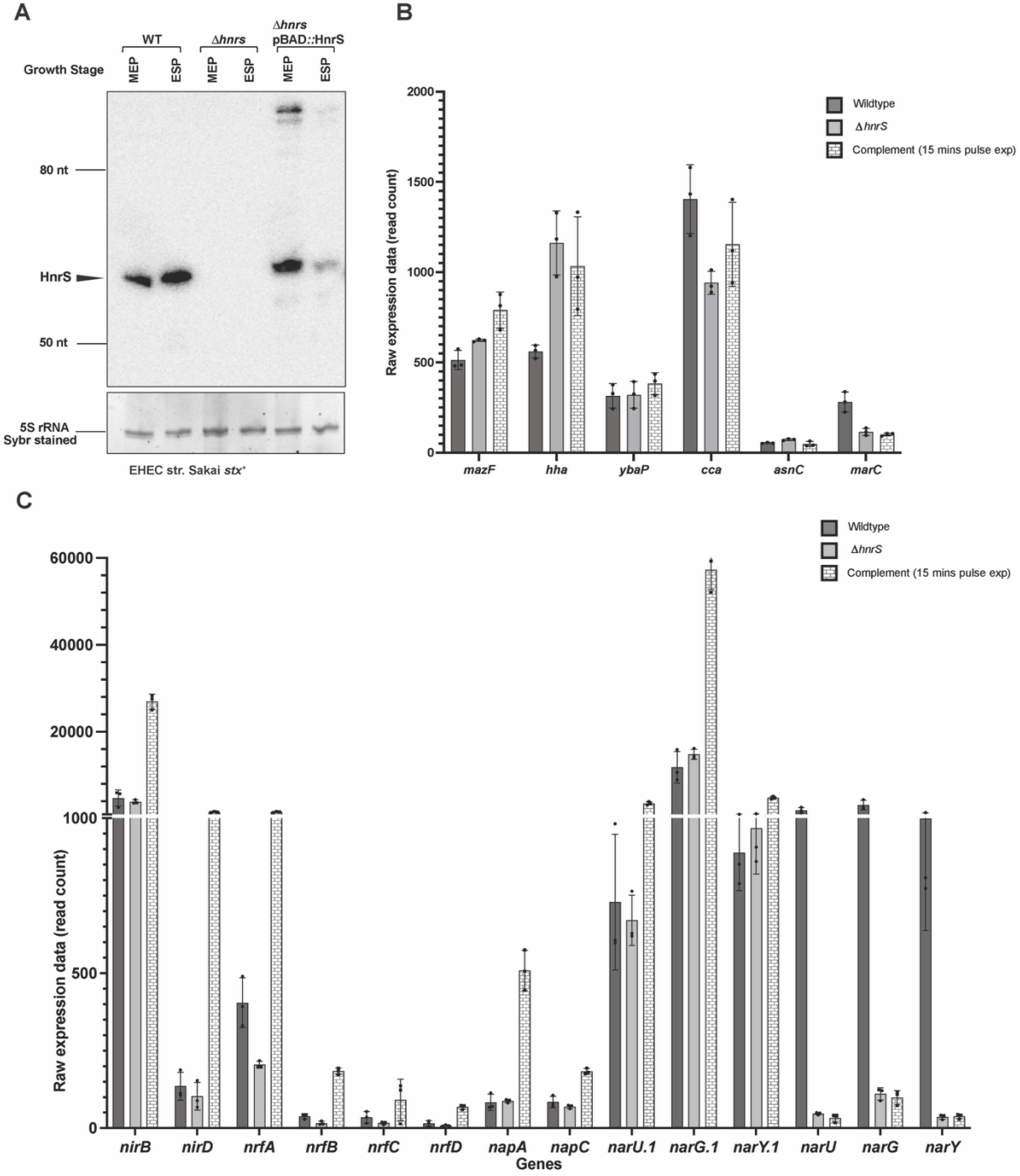
A
WT
Δhnrs
Δhnrs pBAD::HnrS
Growth Stage
MEP
ESP
MEP
ESP
MEP
ESP
80 nt
HnrS
50 nt
5S rRNA Sybr stained
EHEC str. Sakai stx+
B
Wildtype
ΔhnrS
Complement (15 mins pulse exp)
Raw expression data (read count)
2000
1500
1000
500
0
mazF
hha
ybaP
cca
asnC
marC
C
Wildtype
ΔhnrS
Complement (15 mins pulse exp)
Raw expression data (read count)
60000
40000
20000
1000
500
0
nirB
nirD
nrfA
nrfB
nrfC
nrfD
napA
napC
narU.1
narG.1
narY.1
narU
narG
narY
Genes

Supplementary Figure 1

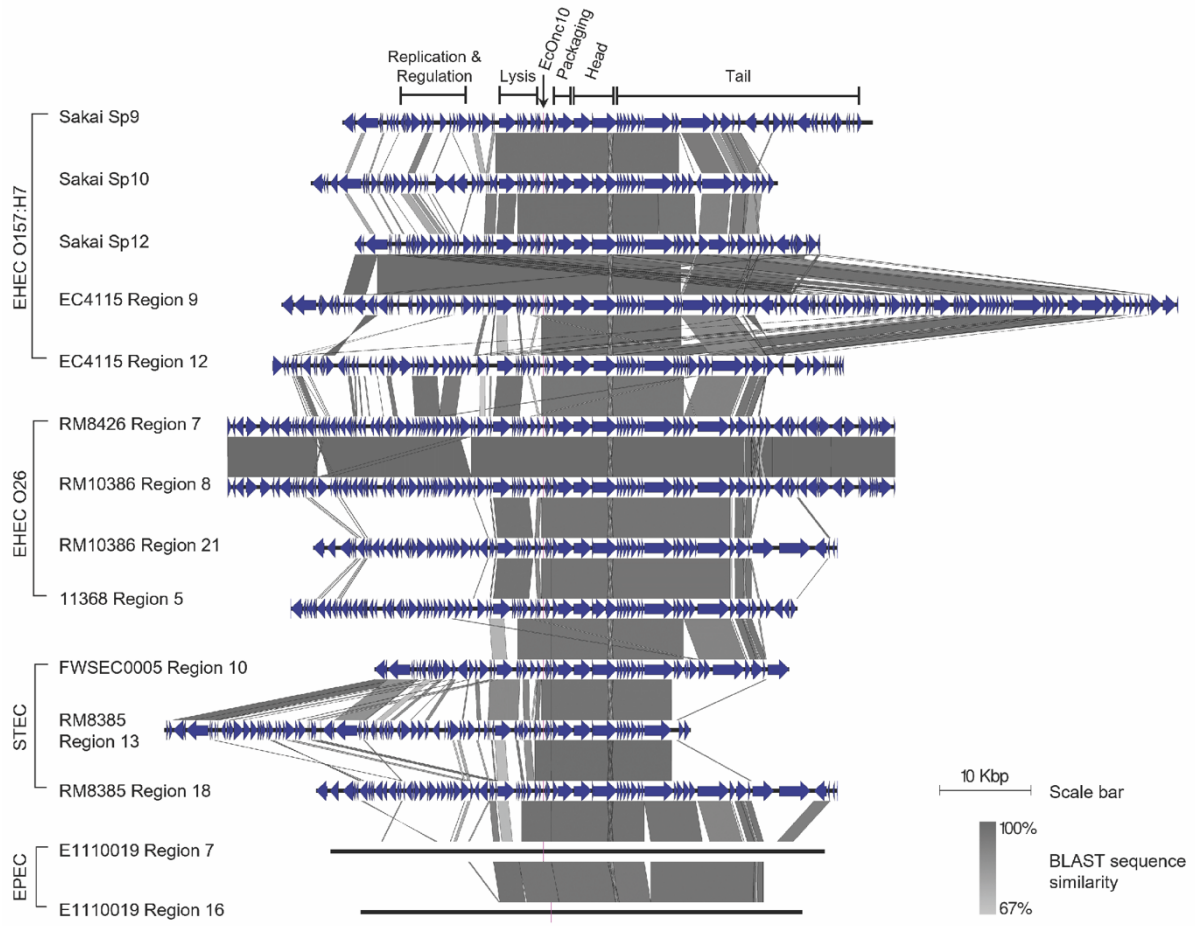

Supplementary Figure 2

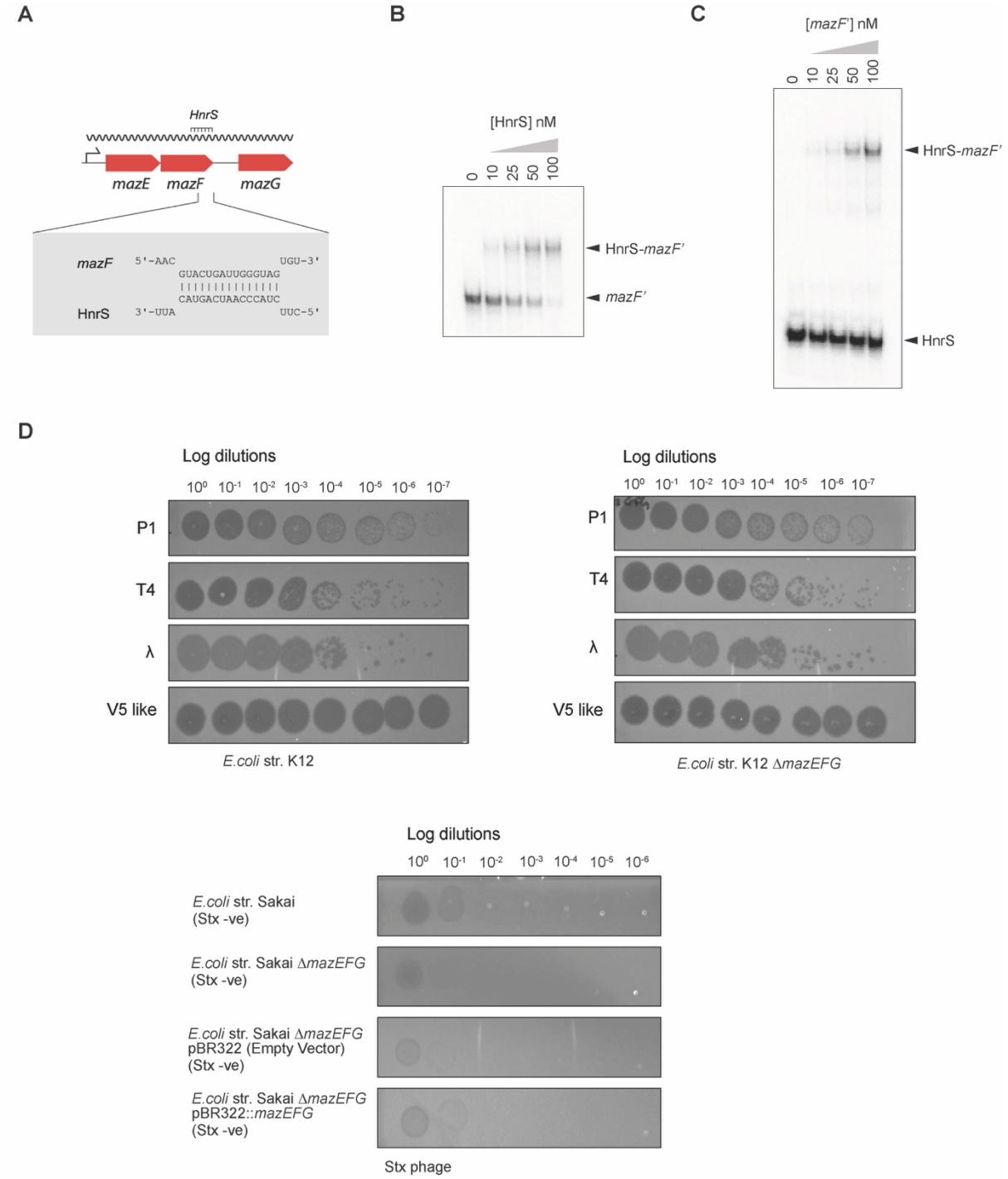

Supplementary Figure 4

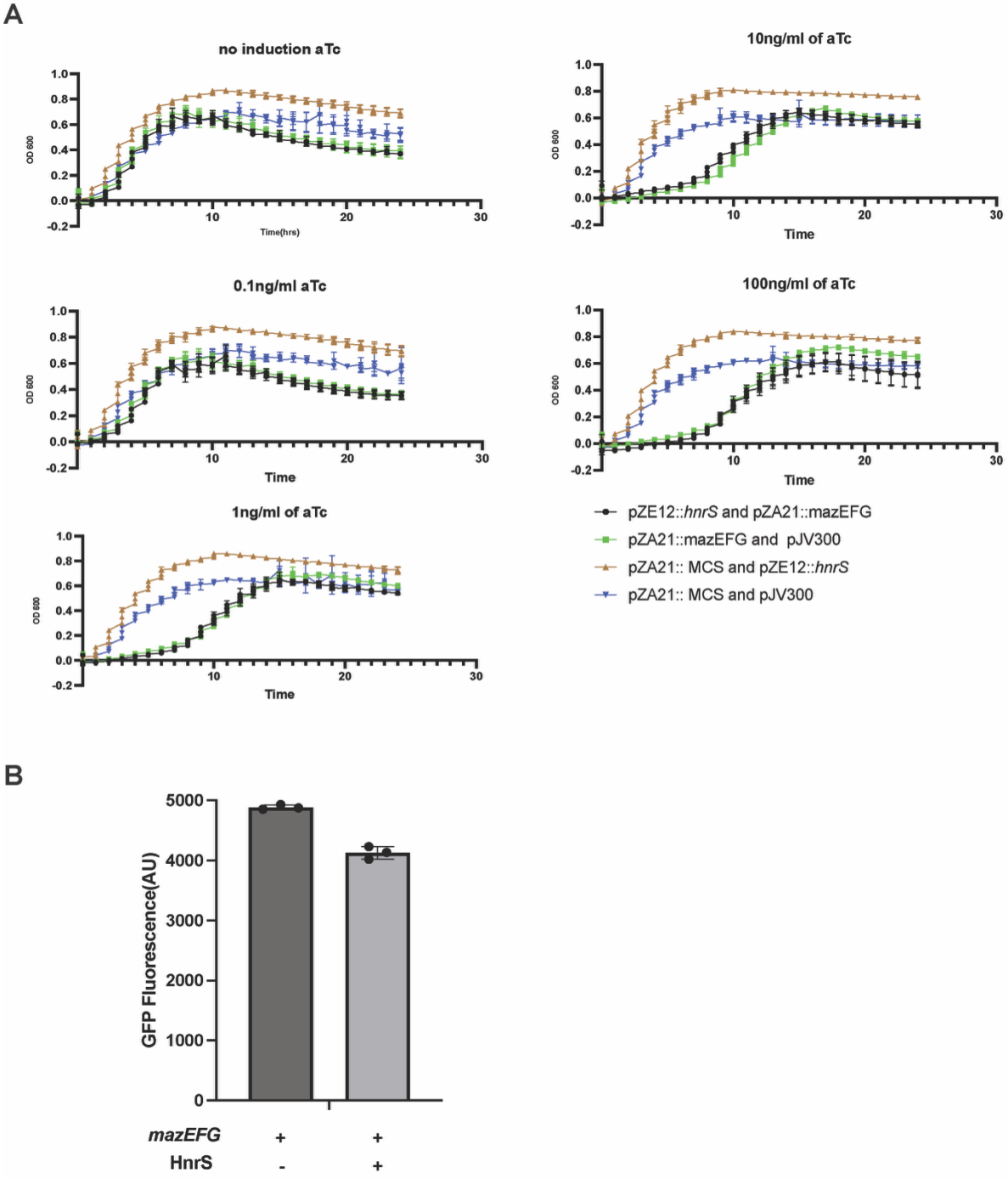

Supplementary Figure 4

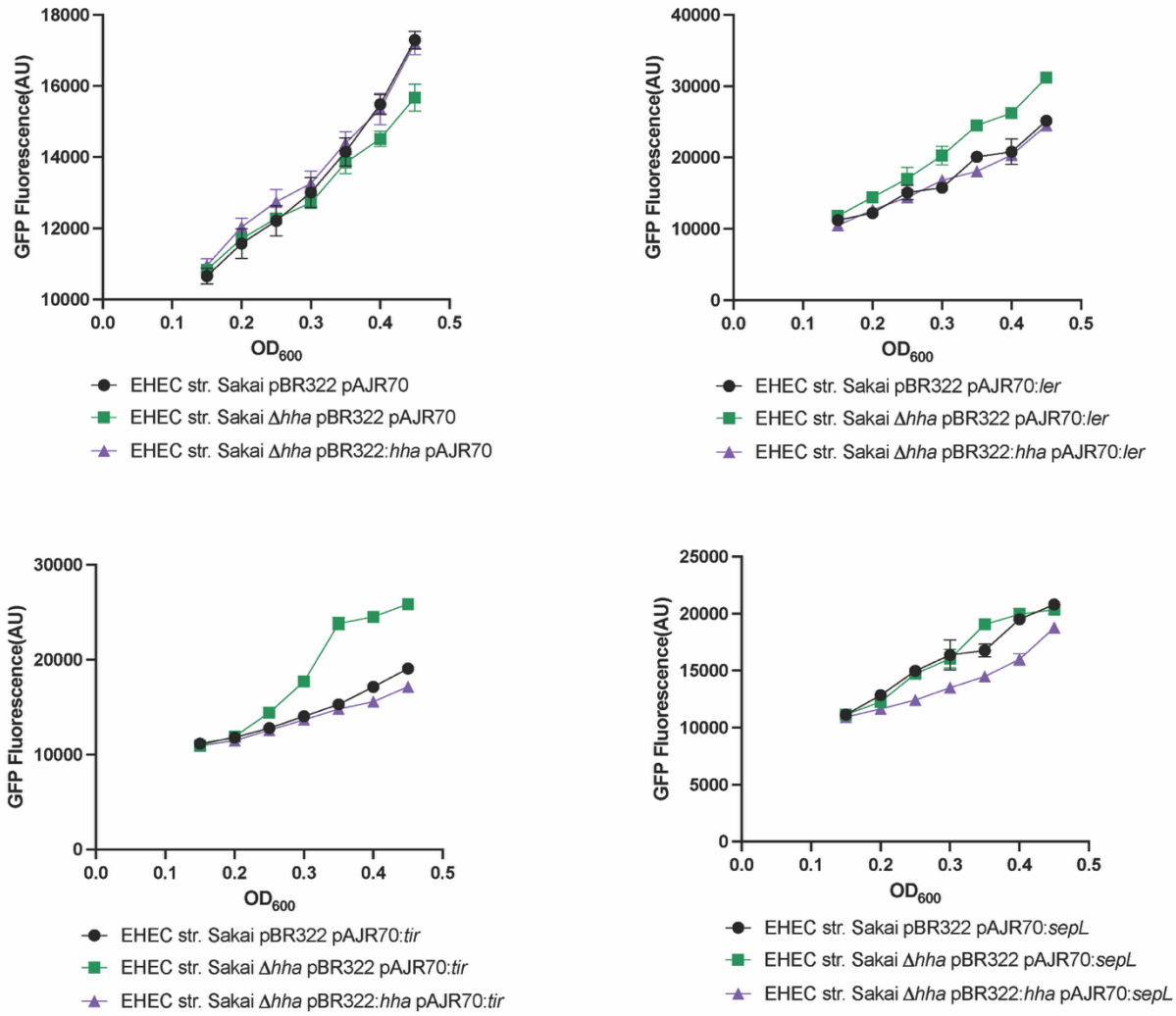

Supplementary Figure 5

A

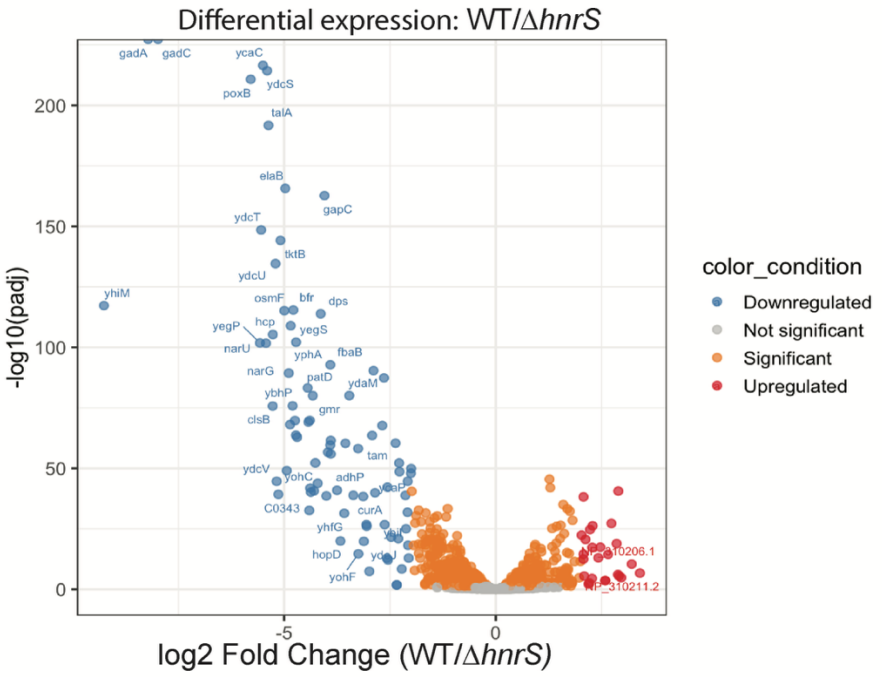

B

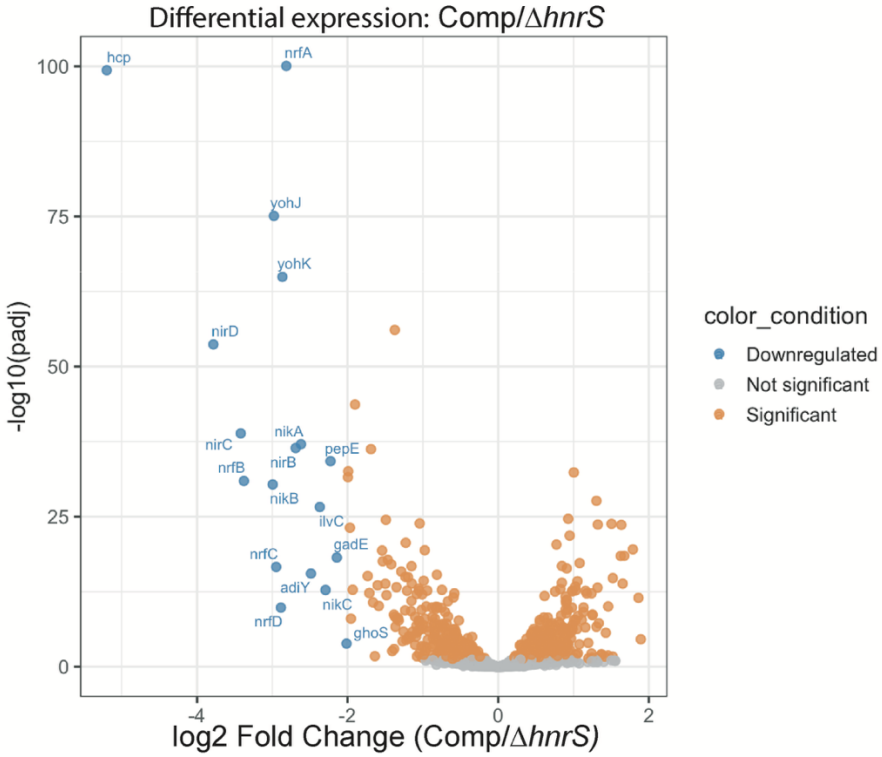

Supplementary Figure 6

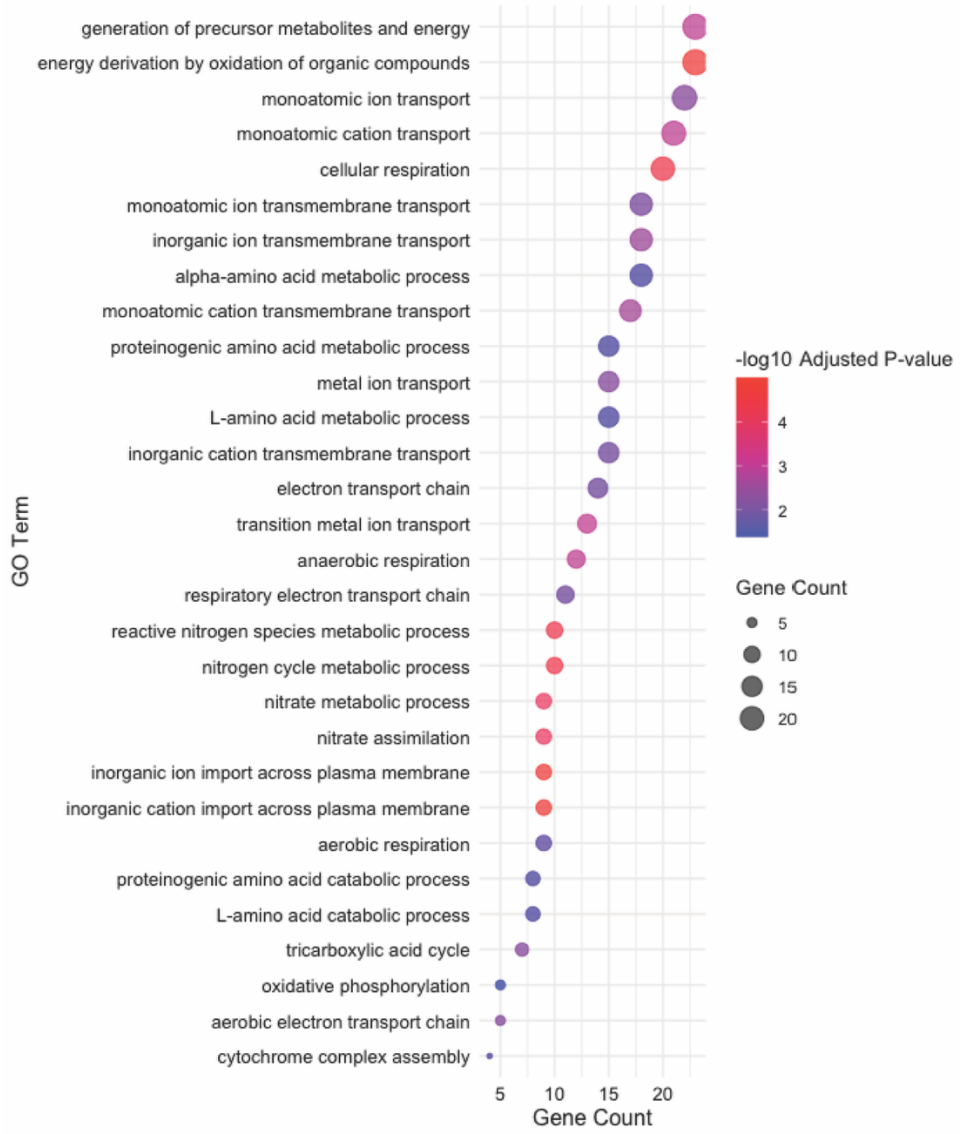

Supplementary Figure 7

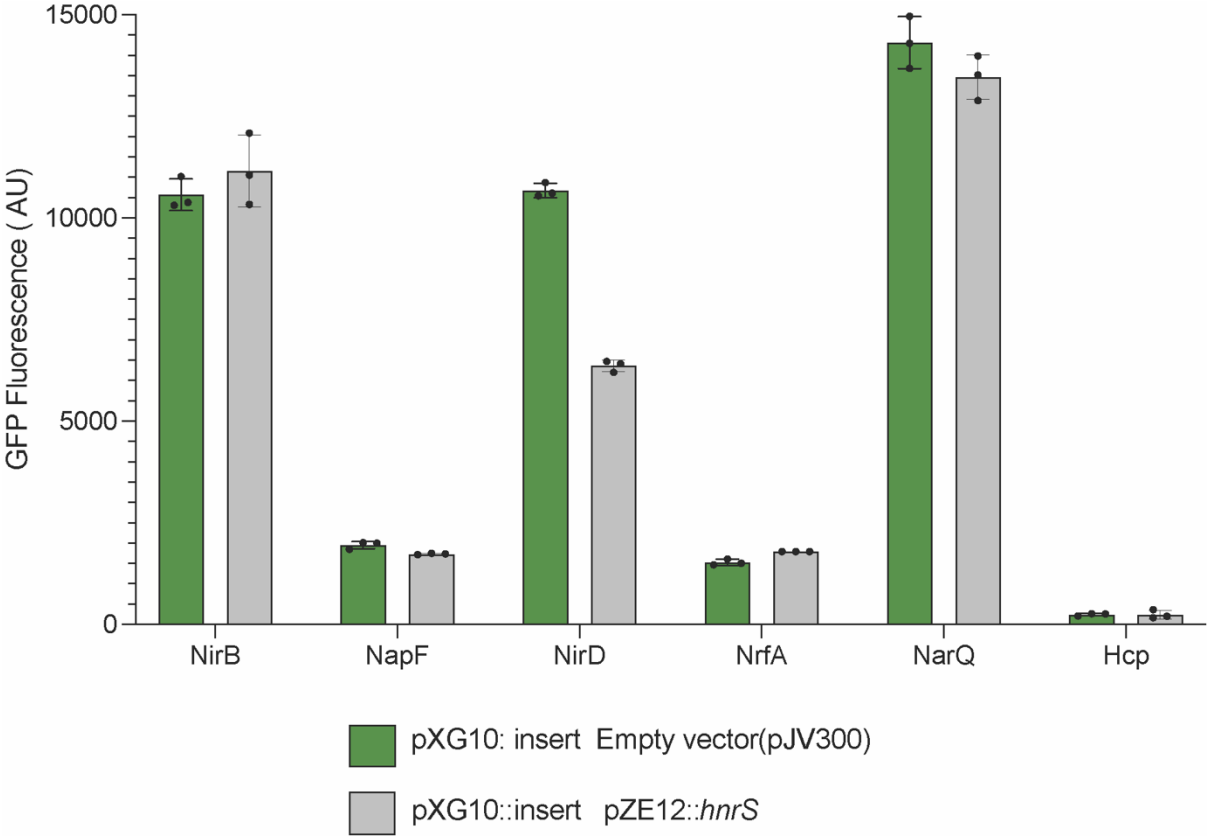
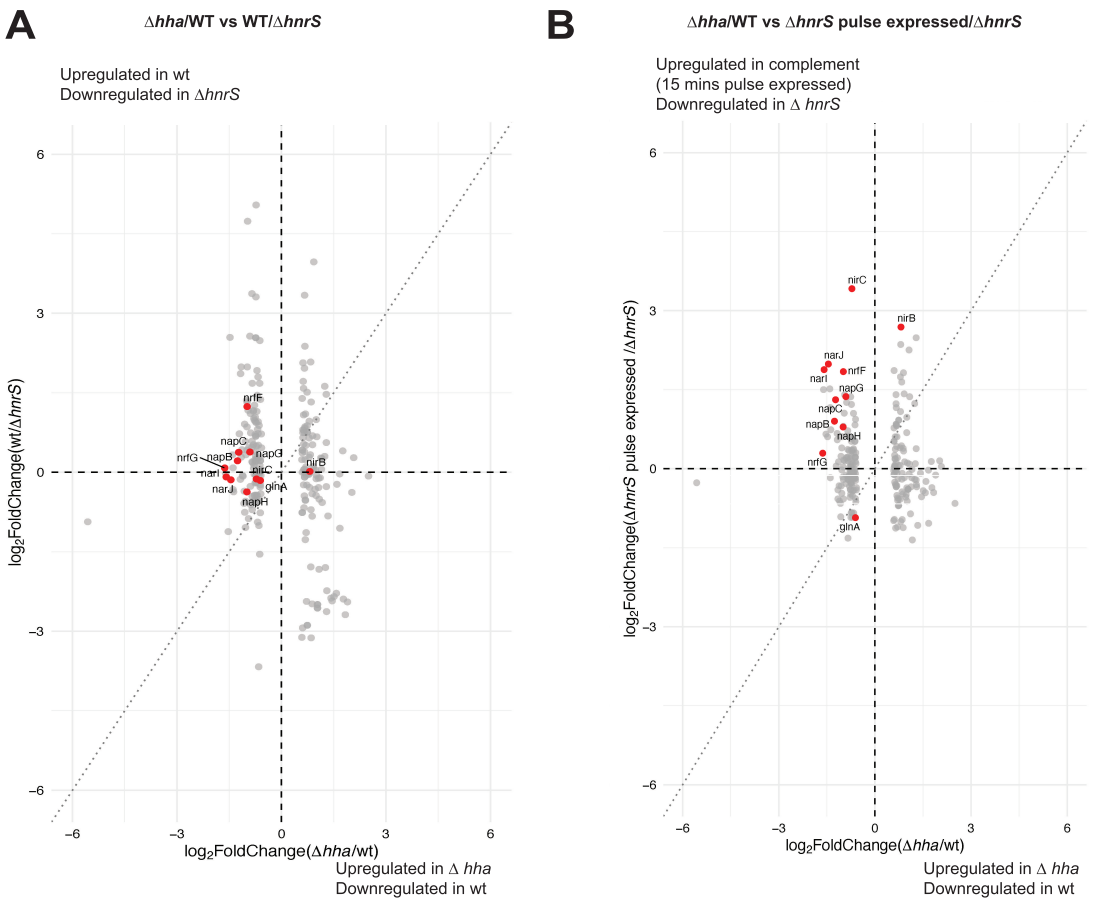
Supplementary Figure 8